Orbitofrontal control of visual cortex gain promotes visual associative learning

Dechen Liu[1,2], Juan Deng[1], Zhewei Zhang[1,2,3], Zhi-Yu Zhang[1,2], Yan-Gang Sun[1,4], Tianming Yang[3,4] and Haishan Yao[1,4*]

[1]Institute of Neuroscience, State Key Laboratory of Neuroscience, CAS Center for Excellence in Brain Science and Intelligence Technology, Chinese Academy of Sciences, Shanghai 200031, China

[2]University of Chinese Academy of Sciences, Beijing 100049, China

[3]Institute of Neuroscience, Key Laboratory of Primate Neurobiology, CAS Center for Excellence in Brain Science and Intelligence Technology, Chinese Academy of Sciences, Shanghai 200031, China

[4]Shanghai Center for Brain Science and Brain-Inspired Intelligence Technology, Shanghai 201210, China

[*] Correspondence: haishanyao@ion.ac.cn

ABSTRACT

Signaling of expected outcomes in the orbitofrontal cortex (OFC) is critical for outcome-guided and learning behavior. The OFC projects to primary visual cortex (V1), yet the function of this top-down projection is unclear. We found that optogenetic activation of OFC projection to V1 reduced the amplitude of V1 visual responses via the recruitment of local somatostatin-expressing (SST) interneurons. Using mice performing a Go/No-Go visual task, we showed that the OFC projection to V1 mediated the suppression of V1 responses to the reward-irrelevant No-Go stimulus. Furthermore, the responses of V1-projecting OFC neurons to No-Go stimulus were reduced when the mice's expectation was incorrect. In addition, optogenetic inactivation of OFC projection to V1 impaired, whereas activation of SST interneurons in V1 improved the learning of Go/No-Go visual task. Thus, OFC top-down projection to V1 is crucial to drive visual associative learning by reducing the response gain of V1 neurons to non-relevant stimulus.

The OFC is a critical brain region for using the information about expected outcomes to guide learning and behavior[1-3]. Studies in rodents and monkeys have demonstrated that the identity and expected values of specific outcomes are represented by activities in the OFC[4-14]. Lesions or inactivation of the OFC impair behavior guided by outcome expectancy and learning driven by the discrepancy

between expected and actual outcomes[15-31], and degrade the acquisition of Pavlovian trace conditioning task[32].

Neural signals in the OFC are used by other brain regions, including the basolateral amygdala (BLA), ventral tegmental area (VTA) and striatum to guide behavior[2,3]. In OFC-lesioned rats, BLA neurons are impaired in the encoding of cue-outcome association and the developing of outcome-expectant activity[33]. The outcome-expectancy signals in the OFC are necessary for VTA dopamine neurons to calculate reward prediction errors[34], which are important teaching signals for reinforcement learning[35,36]. Inactivation of the OFC or disconnection of the OFC from VTA prevents extinction learning in the Pavlovian over-expectation task[25,37]. The VTA-projecting OFC neurons encode long-term memory of cue-reward association, and optogenetic inhibition of these neurons impairs extinction learning and memory[32]. The OFC also connects with sensory cortices[38-40], including V1[38]. It is unknown how the responses of sensory cortex-projecting OFC neurons are modulated by outcome expectancy, and whether the top-down signals from the OFC to sensory cortices influence learning behavior.

Frontal top-down projections to sensory cortices are known to modulate sensory processing[41-44], promote accurate perception[45], and convey predictive signals[46,47]. Associative learning enhances signals related to stimulus expectation or reward expectation in V1, which may be mediated by top-down projections[48]. Learning also enhances the effect of top-down inputs in modulating V1 responses[49]. However, the

causal role of top-down projections to sensory cortices in stimulus-reward associative learning remains unclear.

In this study, we found that activating OFC axons in V1 resulted in suppression of V1 visual response by recruiting SST interneurons. We thus hypothesized that OFC projection to V1 may filter out non-relevant visual information, and tested this hypothesis in mice performing a Go/No-Go visual task. We found that the OFC projection to V1 contributed to the suppression of V1 responses to the No-Go stimulus, which was not associated with reward. Optogenetic tagging of V1-projecting OFC neurons revealed that their responses to the No-Go stimulus were reduced in wrong trials but not in correct trials. We further showed that optogenetic inactivation of OFC projection to V1 slowed the learning of Go/No-Go visual behavior. Thus, the OFC projection to V1 plays a key role in filtering out non-relevant visual information to facilitate associative learning.

Results

OFC top-down projection controls V1 response amplitude by activation of local SST interneurons. We injected Cholera toxin subunit B (CTB) in V1 and found that the retrograde labeled neurons were in the ventrolateral OFC (vlOFC) (Fig. 1a), consistent with the finding in a previous study[38]. By injecting rAAV2-retro-hSyn-Cre in V1 and AAV-DIO-EYFP in the OFC, we found that the axons of OFC neurons terminated in both superficial and deep layers of V1 (Fig. 1b). To examine how the

OFC top-down projection influences V1 neuronal responses, we expressed excitatory opsin Channelrhodopsin-2 (ChR2) or ChrimsonR in the OFC, and measured V1 responses with and without laser stimulation of OFC axons in mice passively viewing drifting gratings (Fig. 1c). Activating OFC axons in V1 significantly reduced the firing rates of V1 neurons in both anesthetized and awake mice (anesthetized mice: $P = 5.2\times10^{-6}$, $n = 102$ neurons; awake mice: $P = 6.53\times10^{-5}$, $n = 62$ neurons; Wilcoxon signed rank test, Fig. 1d). When we computed a rate change index as $(R_{laser\_on} - R_{laser\_off})/(R_{laser\_on} + R_{laser\_off})$, in which R_{laser_on} and R_{laser_off} represented responses averaged over all orientations for laser-on and laser-off trials, respectively, we found that the index was negative for the majority of V1 neurons in both anesthetized and awake mice (Fig. 1e). For control mice injected with AAV-mCherry (or AAV-EGFP) in the OFC, the laser-induced response reduction was significantly smaller than that for mice injected with AAV-ChR2 (or AAV-ChrimsonR) in the OFC (Supplementary Fig. 1a). After blocking antidromic spikings of OFC neurons with tetrodotoxin in the OFC, the response reduction in V1 neurons induced by activating OFC axons was still significant ($P = 2.33\times10^{-12}$, $n = 118$ neurons from awake mice, Wilcoxon signed rank test, Fig. 1f–h), indicating that the laser-induced response reduction was mediated directly by OFC projection to V1, rather than through antidromic activation of indirect pathways. Although the response amplitude was clearly reduced, the orientation selectivity of V1 neurons was not affected by activation of OFC axons in V1 (anesthetized mice: $P = 0.36$, $n = 102$ neurons; awake mice: $P = 0.99$, $n = 62$

88 neurons; Wilcoxon signed rank test, Fig. 1i).

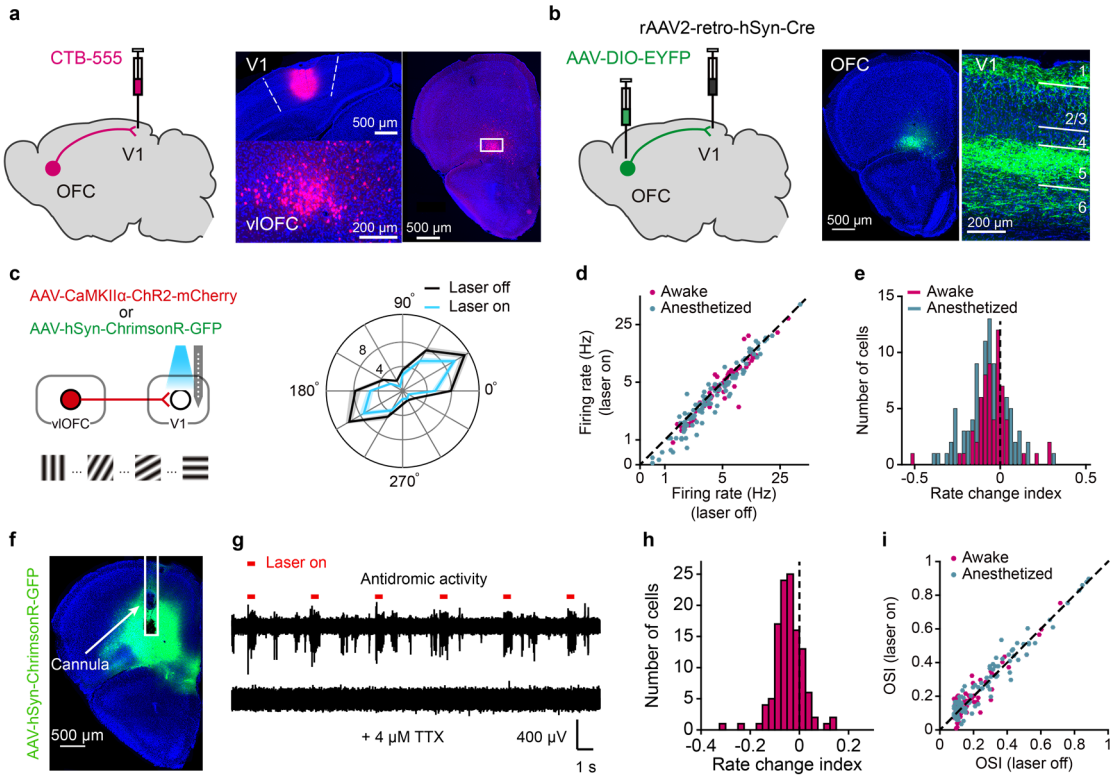

89

90

91 **Fig. 1 | Activating OFC projection to V1 reduces response amplitude of V1**
92 **neurons**. **a**, Left, schematic of CTB injection in V1. Right, Representative
93 fluorescence images of CTB injection in V1 and retrograde labeled neurons in the
94 ventrolateral OFC. **b**, Left, strategy of virus injection to visualize the OFC axons in
95 V1. Right, representative fluorescence images of V1-projecting OFC neurons and
96 their terminals in V1. **c**, Left, schematic of measuring V1 visual responses with and
97 without activating OFC axons in V1. Right, tuning curves of a V1 neuron with (blue)
98 and without (black) laser stimulation of OFC axons in V1. **d**, Mean firing rate (firing
99 rate averaged over all orientations) of V1 neurons with laser on vs. laser off.
100 Anesthetized mice (blue): $P = 5.2\times10^{-6}$, $n = 102$ neurons; awake mice (magenta): $P =$
101 6.53×10^{-5}, $n = 62$ neurons. **e**, Distribution of rate change indexes for V1 neurons in
102 anesthetized ($P = 2.6\times10^{-8}$) and awake mice ($P = 3.81\times10^{-5}$). The rate change index
103 was computed as $(R_{laser\_on} - R_{laser\_off})/(R_{laser\_on} + R_{laser\_off})$, in which R_{laser_on} and R_{laser_off}
104 represented responses averaged over all orientations for laser-on and laser-off trials,
105 respectively. **f**, TTX was infused to the OFC, in which AAV-hSyn-ChrimsonR-GFP
106 had been injected, to block the antidromic spikes induced by laser stimulation in V1.
107 White rectangle shows the placement of the cannula. **g**, TTX infusion into the OFC
108 abolished multi-unit activity in the OFC evoked by laser stimulation in V1. Upper
109 trace, without TTX; Lower trace, with TTX infusion into the OFC. **h**, Distribution of

rate change indexes of V1 neurons recorded with TTX infusion into the OFC. $P = 2.33\times10^{-12}$, $n = 118$ neurons from awake mice. **i**, Orientation selectivity index (OSI) with laser on vs. laser off. Anesthetized mice (blue): $P = 0.36$, $n = 102$; awake mice (magenta): $P = 0.99$, $n = 62$. For **d**, **e**, **h** and **i**, AAV-CaMKIIα-hChR2 (H134R)-mCherry and AAV-hSyn-ChrimsonR-GFP were injected in the OFC for anesthetized and awake mice, respectively. Wilcoxon two-sided signed rank test; shadings and error bars, mean ± s.e.m.

To dissect the circuit mechanism underlying V1 response modulation by the OFC top-down projection, we infected the OFC neurons with AAV-ChR2 and performed whole-cell recordings from V1 neurons in acute slices of V1 containing ChR2-expressing OFC axons. Photostimulation of OFC axons evoked both excitatory and inhibitory postsynaptic currents (EPSCs and IPSCs) in the recorded V1 neurons (Fig. 2a). The onset latencies of the EPSCs were shorter than those of the IPSCs (Fig. 2b), which were blocked by γ-aminobutyric acid type A ($GABA_A$) receptor antagonist picrotoxin (Fig. 2c). We next tested whether IPSCs evoked by activation of OFC axons were feedforward inhibition. We bath applied an α-amino-3-hydroxy-5-methyl-4-isoxazole propionic acid (AMPA) receptor antagonist NBQX, and found that the amplitudes of both EPSCs and IPSCs were reduced (Fig. 2d), indicating that the IPSCs were due to feedforward inhibition generated by local inhibitory neurons in V1. By injecting CTB in V1 of GAD67-GFP mice, we found that the retrograde labeling of OFC neurons did not overlap with the GFP-positive neurons in the OFC (Fig. 2e), confirming that the V1-projecting OFC neurons were not GABAergic.

We next examined which subtype of inhibitory neurons mediates the effect of

activating OFC axons on V1 responses. By using rabies virus (RV)-mediated monosynaptic retrograde tracing[50], we found that V1 interneurons expressing parvalbumin (PV), somatostatin (SST) and vasoactive intestinal peptide (VIP) all received direct innervation from neurons in the vlOFC (Supplementary Fig. 2). Consistently, slice recording showed that optogenetic stimulation of OFC axons evoked EPSCs in three different subtypes of interneurons as well as pyramidal neurons in V1 (Fig. 2f).

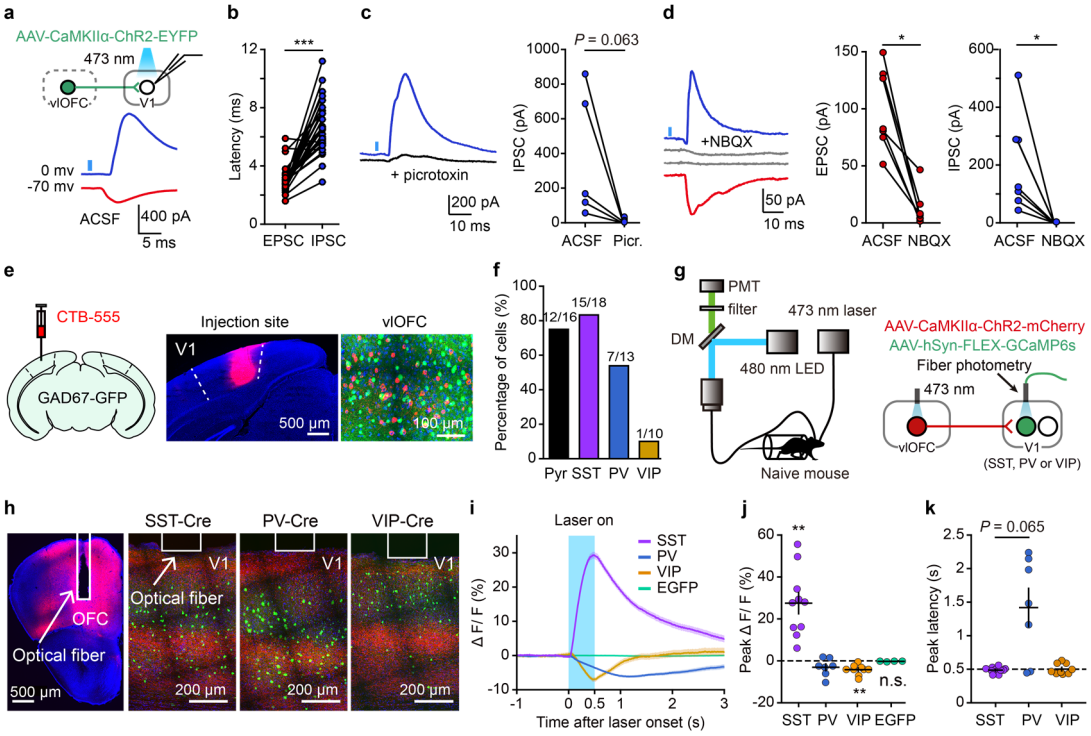

Fig. 2 | Optogenetic activation of OFC axons in V1 activates inhibitory interneurons in V1. a, Photostimulation of OFC projection to V1 evoked both EPSCs (red) and IPSCs (blue) in a V1 neuron. **b**, The onset latencies of laser-evoked EPSCs were significantly shorter than those of IPSCs (***$P = 2.34\times10^{-6}$, $n = 30$, Wilcoxon two-sided signed rank test). **c**, Left, application of a $GABA_A$ receptor antagonist (picrotoxin, 30 μM) blocked IPSCs in a V1 neuron. Black, IPSCs after the application of picrotoxin. Right, comparison of the amplitude of IPSCs before and after picrotoxin application ($P = 0.063$, $n = 5$, Wilcoxon two-sided signed rank test). **d**, Left, application of an AMPA receptor antagonist (NBQX, 10 μM) blocked both

EPSCs and IPSCs in a V1 neuron. Gray, EPSCs and IPSCs after the application of NBQX. Middle and right, comparison of the amplitude of EPSCs (IPSCs) before and after NBQX application ($P = 0.016$ and $n = 7$ for both EPSCs and IPSCs, Wilcoxon two-sided signed rank test). **e**, CTB was injected in V1 of a GAD67-GFP mouse. Retrograde labeling of OFC neurons did not overlap with GFP-positive neurons in the OFC. The experiments were repeated in 3 GAD67-GFP mice. **f**, Fraction of pyramidal (Pyr) and inhibitory interneurons in which EPSCs could be evoked by laser stimulation of OFC axons in V1. PV, SST, or VIP interneurons were identified as tdTomato-expressing neurons in slices from PV::Ai9, SST::Ai9, or VIP::Ai9 mice. **g**, Schematic of the strategy to record activities of specific interneuron type in V1 evoked by OFC activation *in vivo*. **h**, Fluorescence image of OFC in which AAV-CaMKIIα-ChR2-mCherry was injected, and fluorescence images of V1 injected with AAV-hSyn-FLEX-GCaMP6s from a SST-Cre, PV-Cre and VIP-Cre mouse, respectively. White rectangles show the placement of the optic fiber. **i**, Representative ΔF/F signals from a SST-Cre, PV-Cre, VIP-Cre mouse and a C57BL/6 mouse (AAV-hSyn-EGFP injected in V1), respectively. Blue area, period of OFC stimulation. **j**, Amplitude of peak ΔF/F. SST: $P = 0.002$, $n = 10$ mice; PV: $P = 0.078$, $n = 7$ mice; VIP: $P = 0.004$, $n = 9$ mice; EGFP: $P = 0.13$, $n = 4$; Wilcoxon two-sided signed rank test. **k**, Latency of peak ΔF/F. SST vs PV: $P = 0.065$, Wilcoxon two-sided rank sum test. Shadings and error bars, mean ± s.e.m.

We further used fiber photometry to measure the activities of three subtypes of V1 interneuron *in vivo* in response to optogenetic activation of OFC neurons (Fig. 2g). For these mice, we expressed ChR2 in the OFC and calcium indicator GCaMP6s in PV, SST, or VIP interneurons in V1, respectively (Fig. 2h). During the experiment, the mice were awake but were not viewing visual stimulus. We found that optogenetic activation of OFC neurons caused increase in calcium signals in SST interneurons, but reduction in calcium signals in PV and VIP interneurons in V1 (Fig. 2i, j). Since the latency of laser-evoked peak responses for PV interneurons was longer than that for SST interneurons (Fig. 2k), the reduced PV neuronal responses are likely to be attributed to inhibition caused by SST interneuron activation[51]. Early activated

183 population of SST interneurons could also inhibit VIP interneurons[51], causing their
184 activity reduction. Therefore, OFC stimulation *in vivo* preferentially activated SST
185 interneurons in V1, providing a circuit mechanism for top-down modulation of V1
186 responses by the OFC.
187
188 **OFC projection to V1 mediates the suppression of V1 responses to non-relevant**
189 **visual stimulus.** To examine whether inactivating the OFC projection to V1
190 influences V1 neuronal responses, we expressed inhibitory opsin Jaws in the OFC. By
191 recording V1 neurons from awake mice passively viewing drifting gratings, we found
192 that inactivating the OFC projection to V1 did not cause significant change in V1
193 responses as compared to the control mice ($P = 0.17$, Wilcoxon rank sum test,
194 Supplementary Fig. 1b, c).
195 We next wondered whether the OFC projection to V1 may function during task
196 engagement to suppression V1 responses to non-relevant visual stimulus. To test this
197 hypothesis, we trained head-fixed mice to perform a Go/No-Go visual task (Fig. 3a,
198 b), in which a vertical grating (the "Go" stimulus) and a horizontal grating (the "No-
199 Go" stimulus) were associated with water reward and no reward, respectively. In each
200 trial, the duration of stimulus presentation included a waiting period, during which
201 licking had no consequence, and an answer period (Fig. 3a). For a Go trial, licking
202 within the answer period was rewarded with water (hit). For a No-Go trial, licking
203 (false alarm, FA) within the answer period was neither rewarded nor punished, and

withholding licking within the answer period represented correct rejection (CR). During the inter-trial interval (ITI), the screen was blank and licking was punished with a longer ITI. The training of the Go/No-Go task was preceded by 2 sessions of conditioning, in which the mouse learned to lick within the answer period after the presentation of a Go stimulus. We found that the latency of the first lick after stimulus onset increased with training, and the ITI decreased over sessions (Supplementary Fig. 3), indicating that the mice gradually understood the task structure. Over 11 training sessions (one session per day) of the Go/No-Go task, the hit rate remained high throughout all sessions, whereas the CR rate and discriminability (d') increased with days of training (Fig. 3c, d). Thus, the learning of the task depended on the improvement of CR for the reward-irrelevant No-Go stimulus.

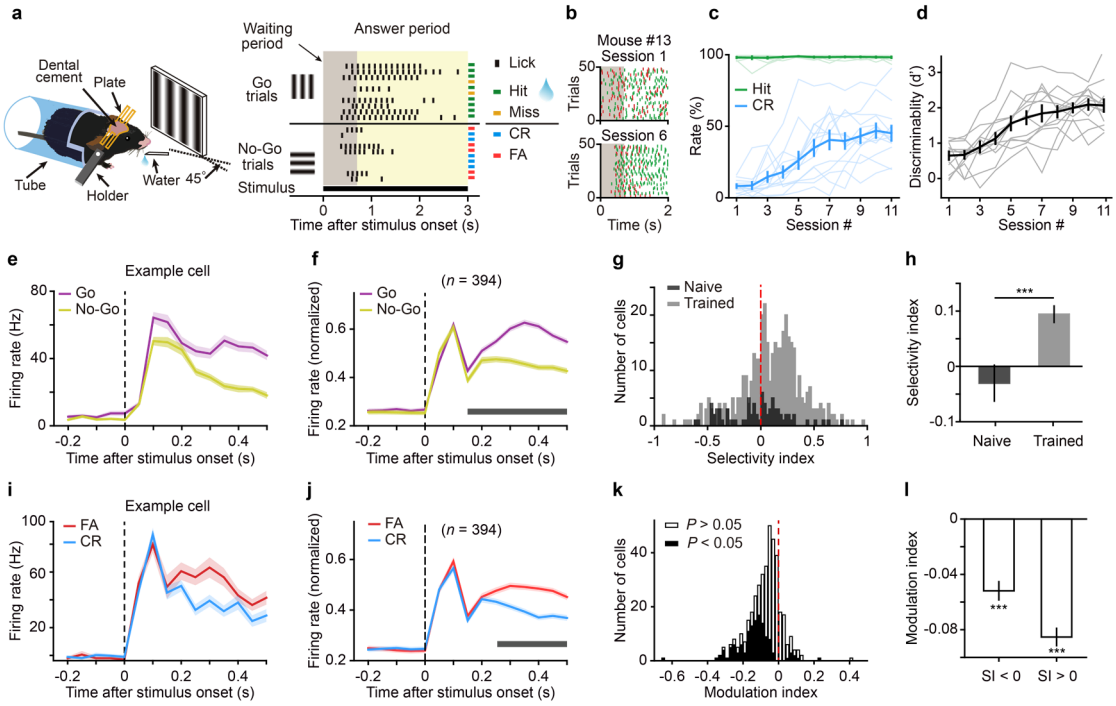

Fig. 3 | Responses of V1 neurons in Go/No-Go visual task. a, Left, behavioral

setup. Right, schematic of task structure. In each trial, the duration of stimulus presentation included a waiting period (gray) and an answer period (yellow). CR, correct rejection. FA, false alarm. **b**, Lick rasters from a subset of trials in two behavioural sessions for a mouse. Green, hit; red, FA. Gray, waiting period. **c**, Hit (green) and CR rates (blue) over sessions (n = 13 mice). Each thin line represents a mouse. For hit rate, $F_{(2.72, 32.62)} = 0.43$, $P = 0.71$; for CR rate, $F_{(3.36, 40.28)} = 23.57$, $P = 2.1\times10^{-9}$. **d**, Discriminability over sessions. Each thin line represents a mouse. $F_{(4.49, 53.86)} = 33.34$, $P = 1.1\times10^{-14}$. One-way repeated measures ANOVA with the Greenhouse-Geisser correction. **e**, Responses of an example V1 neuron to the Go and No-Go stimuli. **f**, The firing rates of each V1 neuron were normalized by the maximum of the peak values in the Go and No-Go trials, and were averaged across neurons. Horizontal bar indicates time points in which the responses between Go and No-Go trials were significantly different ($P < 0.05$, two-way repeated measures ANOVA $F_{(1, 393)} = 55.7$, $P = 5.5\times10^{-13}$ followed by Sidak's multiple comparisons test). **g**, Distribution of selectivity indexes for V1 neurons. Light gray, trained mice, $P = 2.2\times10^{-12}$, n = 394 neurons. Dark gray, naive mice, $P = 0.41$, n = 78 neurons. Wilcoxon two-sided signed rank test. **h**, Comparison of selectivity indexes between V1 neurons in naive and trained mice. *** $P = 1.4\times10^{-4}$, Wilcoxon two-sided rank sum test. **i**, Responses of an example V1 neuron to the No-Go stimulus in FA and CR trials. **j**, The firing rates of each V1 neuron to the No-Go stimulus were normalized by the maximum of the peak values in FA and CR trials, and were averaged across neurons. Horizontal bar indicates time points in which the responses between FA and CR conditions were significantly different ($P < 0.05$, two-way repeated measures ANOVA $F_{(1, 393)} = 222.22$, $P < 1\times10^{-15}$ followed by Sidak's multiple comparisons test). **k**, Distribution of modulation indexes (MIs) for V1 neurons ($P = 1.46\times10^{-42}$, n = 394 neurons, Wilcoxon two-sided signed rank test). **l**, The MIs for V1 neurons preferring the Go stimulus (SI > 0, n = 270) and preferring the No-Go stimulus (SI < 0, n = 124) were both significantly smaller than zero (***$P < 2\times10^{-10}$, Wilcoxon two-sided signed rank test).

We performed single-unit extracellular recordings from V1 in behaving mice that had been trained for at least 5 days. We first compared the responses of V1 neurons to the Go and No-Go stimuli (Fig. 3e, f). We defined a selectivity index (SI) as $(R_{Go} - R_{No\text{-}Go})/(R_{Go} + R_{No\text{-}Go})$, in which R_{Go} and $R_{No\text{-}Go}$ are firing rates to the Go and No-Go stimuli during the waiting period, respectively. The SIs of V1 neurons were

253 significantly larger than zero ($P = 2.2\times10^{-12}$, Wilcoxon signed rank test, Fig. 3g) and
254 significantly larger than those in naive mice ($P = 1.4\times10^{-4}$, $n = 394$ neurons from
255 trained mice and 78 neurons from naive mice, Wilcoxon rank sum test, Fig. 3g, h),
256 indicating a predominant preference for the Go stimulus, consistent with previous
257 reports[48,52]. We also compared the responses of V1 neurons to the No-Go stimulus
258 between correct and wrong trials (Fig. 3i, j). We defined a modulation index (MI) as
259 $(R_{CR} - R_{FA})/(R_{CR} + R_{FA})$, in which R_{CR} and R_{FA} are firing rates to the No-Go stimulus
260 during the waiting period in CR and FA trials, respectively. We found that the MIs
261 were significantly smaller than zero for the population of V1 neurons ($P = 1.46\times10^{-42}$,
262 $n = 394$ neurons, Wilcoxon signed rank test, Fig. 3k). For neurons preferring the Go
263 stimulus ($SI > 0$, $n = 270$) and those preferring the No-Go stimulus ($SI < 0$, $n = 124$),
264 the MIs were both significantly smaller than zero (Fig. 3l). Thus, the responses of V1
265 neurons to the No-Go stimulus during the waiting period were lower in CR than in FA
266 trials.

267 The stimulus selectivity and response modulation of V1 neurons during the
268 waiting period could be attributed to multiple factors, including movement, reward
269 expectation and top-down modulation[48,53]. We next examined whether the OFC top-
270 down projection plays a role in the modulation of V1 responses to stimuli in the
271 Go/No-Go task. We expressed inhibitory opsin Jaws in the OFC, and recorded from
272 V1 neurons with and without optogenetic inactivation of OFC projection to V1 in
273 behaving mice. Laser stimulation was turned on 100-ms before or at stimulus onset,

274 covering the duration of stimulus presentation, and laser-on and laser-off blocks were
275 interleaved. For one group of mice, laser stimulation was applied during Go trials
276 (Fig. 4 a–d). We found that inactivating OFC axons in V1 during Go trials did not
277 affect V1 responses to the Go stimulus during the waiting period (Fig. 4c), nor the
278 behavioral performance (hit rate and CR rate) of the mice (Fig. 4d). For another group
279 of mice, laser stimulation was applied during No-Go trials (Fig. 4e–l). Inactivating
280 OFC axons during No-Go trials significantly increased the responses of V1 neurons to
281 the No-Go stimulus during the waiting period ($P = 0.01$, $n = 169$ neurons, Wilcoxon
282 signed rank test), resulting in a significant reduction of SI ($P = 0.007$, Wilcoxon
283 signed rank test, Fig. 4f). The increase of response to the No-Go stimulus was
284 significant in CR but not in FA trials (CR: $P = 1.02\times10^{-6}$; FA: $P = 0.66$, $n = 169$
285 neurons, Wilcoxon signed rank test, Fig. 4h), leading to a reduction in the amplitude
286 of MI ($P = 6.4\times10^{-4}$, Wilcoxon signed rank test, Fig. 4i). Such effect was observed in
287 both experiments in which laser stimulation was turned on 100-ms before stimulus
288 onset (Supplementary Fig. 4a–c) and at stimulus onset (Supplementary Fig. 4e–g). As
289 laser stimulation during No-Go trials did not affect the mice's lick rate or orofacial
290 movement during the waiting period in CR trials (Fig. 4j, k, Supplementary Fig. 5 and
291 Supplementary Video 1), the laser-induced response increase in CR trials could not be
292 accounted for by a change in movement. Although inactivating OFC axons during
293 No-Go trials significantly influenced the responses of V1 neurons to the No-Go
294 stimulus, it did not change the performance of the mice (Fig. 4l). For control mice that

295 GFP was expressed in the OFC, laser stimulation during No-Go trials did not
296 significantly change the responses of V1 neurons to the No-Go stimulus in either CR
297 or FA trials (Supplementary Fig. 4i, j). Thus, the activity of OFC projection to V1
298 contributes to the suppression of V1 responses to the reward-irrelevant No-Go
299 stimulus in correct trials.

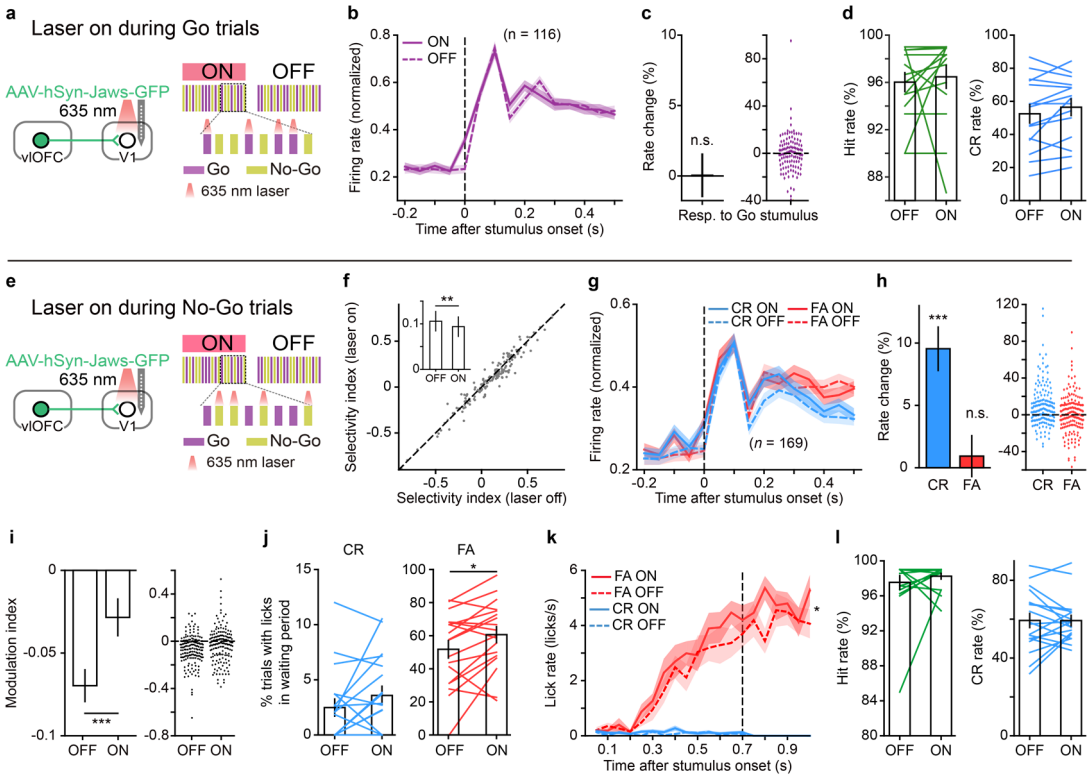

300
301
302 **Fig. 4 | Optogenetic inactivation of OFC projection to V1 during No-Go trials**
303 **increases V1 responses to No-Go stimulus in CR condition. a–d**, Laser stimulation
304 was applied during Go trials. **a**, Left, strategy for inactivating OFC projection to V1.
305 Right, schematic of laser stimulation. **b**, Normalized responses to the Go stimulus
306 with and without inactivating OFC axons in V1. **c**, Inactivating OFC axons in V1
307 during Go trials did not affect V1 responses to the Go stimulus. $P = 0.87$, $n = 116$
308 neurons. The rate change was computed as $(R_{laser\_on} - R_{laser\_off})/R_{laser\_off}$, where R_{laser_on}
309 and R_{laser_off} represented waiting-period firing rates to the Go stimulus with and
310 without laser stimulation, respectively. **d**, Inactivating OFC axons in V1 during Go
311 trials did not affect the hit rate ($P = 0.26$) or the CR rate of the mice ($P = 0.11$, $n = 15$
312 sessions from 7 mice). **e–l**, Laser stimulation was applied during No-Go trials. **e**,
313 Strategy for inactivating OFC projection to V1 and schematic of laser stimulation. **f**,

Inactivating OFC axons in V1 during No-Go trials significantly reduced the selectivity index of V1 neurons (**P = 0.007, n = 169). **g**, Normalized responses to the No-Go stimulus in FA and CR trials, respectively, with and without inactivating OFC axons in V1. **h**, Inactivating OFC axons in V1 during No-Go trials increased the responses of V1 neurons in CR (***$P = 1.02\times10^{-6}$) but not in FA trials (P = 0.66). n = 169 neurons. For CR condition, the rate change was computed as ($R_{CR\_laser\_on}$ - $R_{CR\_laser\_off}$)/$R_{CR\_laser\_off}$, where $R_{CR\_laser\_on}$ and $R_{CR\_laser\_off}$ represented delay-period firing rates to No-Go stimulus in CR trials with and without laser stimulation, respectively. For FA condition, the rate change was computed as ($R_{FA\_laser\_on}$ - $R_{FA\_laser\_off}$)/$R_{FA\_laser\_off}$, where $R_{FA\_laser\_on}$ and $R_{FA\_laser\_off}$ represented delay-period firing rates to No-Go stimulus in FA trials with and without laser stimulation, respectively. **i**, Inactivating OFC axons in V1 during No-Go trials significantly reduced the amplitude of MI (***$P = 6.4\times10^{-4}$, n = 169 neurons). **j**, Inactivating OFC axons in V1 during No-Go trials increased the percentage of FA trials in which licks occurred within the waiting period (P = 0.02), but did not significantly change the percentage of CR trials in which licks occurred within the waiting period (P = 0.14, n = 18 sessions from 14 mice). **k**, Inactivating OFC axons in V1 during No-Go trials significantly increased the lick rate during waiting period of FA trials (two-way repeated measures ANOVA $F_{(1, 17)} = 7.78$, P = 0.01) but did not significantly change the lick rate during waiting period of CR trials (two-way repeated measures ANOVA $F_{(1, 17)} = 1.6$, P = 0.22). **l**, Inactivating OFC axons in V1 during No-Go trials did not affect the hit rate (P = 0.56) or the CR rate of the mice (P = 0.95, n = 18 sessions from 14 mice). Wilcoxon two-sided signed rank test for **c**, **d**, **f**, **h**, **i**, **j**, **l**. Shadings and error bars, mean ± s.e.m.

V1-projecting OFC neurons show response reduction during expectation of reward. Next, we sought to identify V1-projecting OFC neurons with optogenetic tagging method and examined their responses during the Go/No-Go visual task. To this end, we first injected rAAV2-retro-hSyn-ChrimsonR-GFP[54] in V1, resulting in the expression of excitatory opsin ChrimsonR in V1-projecting OFC neurons (Supplementary Fig. 6). We performed extracellular recordings from the OFC to monitor the spikes evoked by red laser stimulation (Fig. 5a, b). Using stimulus-associated spike latency test (SALT) for optogenetic identification[55], we identified

V1-projecting OFC neurons as those showing significant laser-evoked responses with short latencies (n = 22 out of 1175 units, $P < 0.01$, Fig. 5c, d and Supplementary Fig. 6f). In mice that had been trained for at least 6 days, the responses of identified OFC neurons to the Go and No-Go stimuli were monitored during the behavioral task (Fig. 5e). We defined a response index (RI) as $(R_{evoked} - R_{baseline})/(R_{evoked} + R_{baseline})$, where R_{evoked} and $R_{baseline}$ represented the firing rates during the waiting period and the baseline period before stimulus onset, respectively. For each neuron, we computed RIs for the responses to the Go stimulus in hit trials and those to the No-Go stimulus in CR (or FA) trials, respectively. We found that the RIs in hit and FA trials were both significantly smaller than zero, whereas the RIs in CR trials were not significantly different from zero (Supplementary Fig. 6). Thus, the responses to the Go stimulus in hit trials and those to the No-Go stimulus in FA trials were reduced, as compared to the baseline responses, whereas those to the No-Go stimulus in CR trials were unchanged. During the behavioral sessions of OFC recordings, the mice showed anticipatory licking during the waiting period for the No-Go stimulus in FA trials as well as for the Go stimulus in hit trials (Supplementary Fig. 6). These results suggest that V1-projecting OFC neurons reduced firing when the mice expected reward. For V1-projecting OFC neurons, the responses to the No-Go stimulus were significantly lower in FA than in CR trials (Fig. 5f), and MIs were significantly larger than zero ($P = 6.9\times10^{-4}$, $n = 22$ neurons, Wilcoxon signed rank test, Fig. 5g), suggesting that their responses the No-Go stimulus were reduced when the mice's expectation was

incorrect. As the spike rate of V1-projecting OFC neurons was not correlated with the lick rate (Supplementary Fig. 6k), the response difference between CR and FA trials could not be attributed to licking. Given that activating OFC axons in V1 caused response suppression of V1 neurons (Fig. 1), the higher responses of V1-projecting OFC neurons in CR than in FA trials (Fig. 5f, g) may provide an explanation of the observation that V1 responses to the No-Go stimulus were lower in CR trials (Fig. 3j, k).

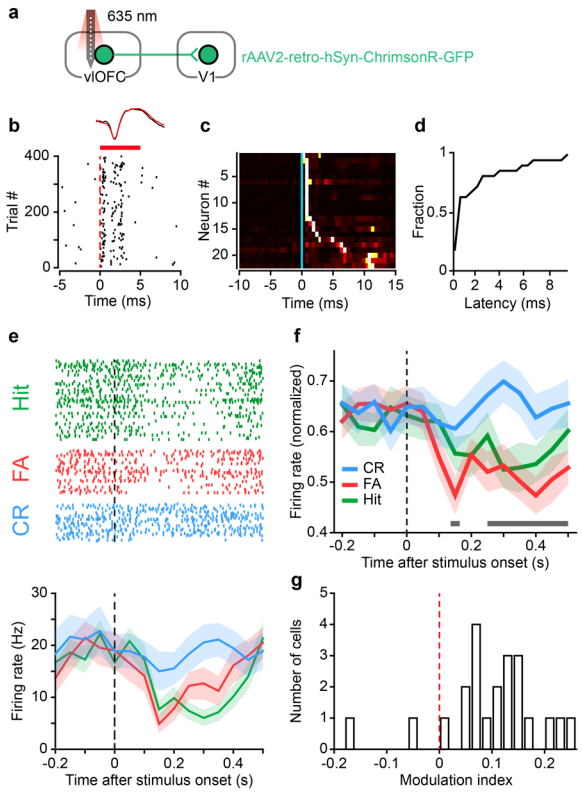

Fig. 5 | V1-projecting OFC neurons show response reduction during expectation of reward. a, Schematic of the strategy for phototagging V1-projecting OFC neurons. **b**, Spike raster of an identified V1-projecting OFC neuron aligned to laser onset. Red bar, duration of laser stimulation. Top, mean waveforms for spontaneous (black) and laser-evoked (red) spikes. **c**, PSTHs aligned to laser onset (blue line) for all identified neurons. The responses were normalized by peak value and sorted by peak latency.

Colors from black to white indicate increase in firing rate. **d**, Cumulative distribution of laser-evoked spike latency for all identified neurons. **e**, Spike rasters and PSTHs of an identified V1-projecting OFC neuron during hit (green), FA (red) and CR (blue) trials, aligned to stimulus onset. **f**, The firing rates of each neuron were normalized by the maximum of the peak values in hit, FA, and CR trials, and were averaged across neurons. Horizontal bar indicates time points in which the responses between FA and CR conditions were significantly different ($P < 0.05$, two-way repeated measures ANOVA $F_{(1, 21)} = 17.86$, $P = 3.79\times10^{-4}$ followed by Sidak's multiple comparisons test). **g**, Distribution of MIs for identified V1-projecting OFC neurons. $P = 6.9\times10^{-4}$, $n = 22$ neurons, Wilcoxon two-sided signed rank test. Shadings, mean ± s.e.m.

OFC projection to V1 contributes to visual associative learning. The above results showed that, although inactivating OFC projection to V1 could affect V1 responses, it did not change the behavioral performance of mice (Fig. 4l). As these mice had been trained before the optogenetic perturbation, we next examined whether perturbation of OFC projection to V1 from the first day of training influences the learning process. To inactivate the OFC projection to V1, we expressed Jaws in the OFC (Fig. 6a and Supplementary Fig. 7). For control mice, EGFP alone was expressed in the OFC (Fig. 6a). Both the Jaws-expressing and the EGFP-expressing mice were divided into two groups. The laser stimulation was applied to V1 during No-Go trials for one group (Fig. 6b–d) and during Go trials for another group (Fig. 6e–g). Throughout the learning process, each session consisted of interleaved blocks of laser-on and laser-off trials. For the group of Jaws-expressing mice with laser stimulation during No-Go trials, the behavioral performance were similar between laser-on and laser-off trials (Fig. 6b), indicating that inactivation of the OFC axons in V1 during No-Go trials did not affect the immediate performance and corroborating the result in Fig. 4l.

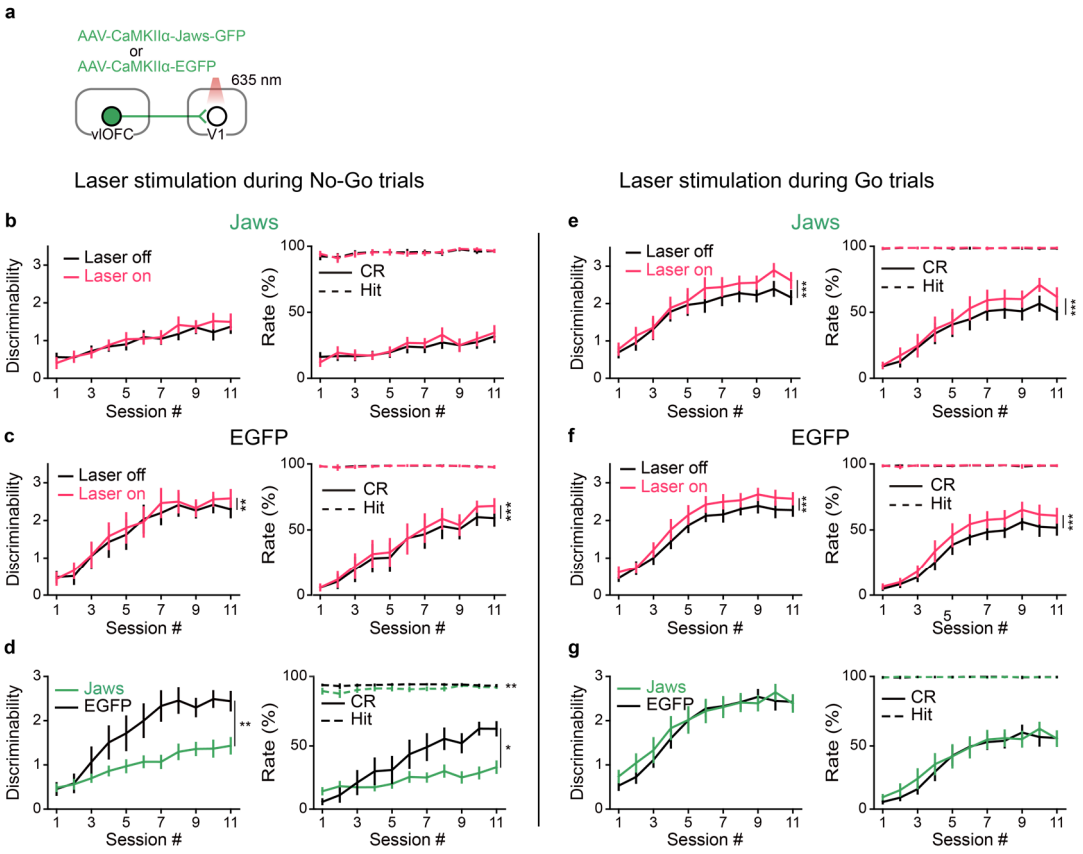

Fig. 6 | Inactivating OFC projection to V1 during No-Go trials slows the learning of Go/No-Go visual task. a, Schematic of the strategy for inactivating OFC projection to V1. **b–d**, Laser stimulation was applied during No-Go trials. **b**, Discriminability (left), hit and CR rates (right) with and without laser stimulation during No-Go trials for mice in which AAV-CaMKIIα-Jaws-GFP was injected in the OFC (n = 13). Discriminability: $F_{(1, 12)} = 1.77$, $P = 0.21$; hit rate: $F_{(1, 12)} = 0.06$, $P = 0.81$; CR rate: $F_{(1, 12)} = 3.44$, $P = 0.09$. Two-way repeated measures ANOVA. **c**, Discriminability, hit and CR rates with and without laser stimulation during No-Go trials for control mice in which AAV-CaMKIIα-EGFP was injected in the OFC (n = 9). Discriminability: $F_{(1, 8)} = 20.98$, $P = 0.002$; hit rate: $F_{(1, 8)} = 0.55$, $P = 0.48$; CR rate: $F_{(1, 8)} = 31.32$, $P = 5.13\times10^{-4}$. Two-way repeated measures ANOVA. **d**, Effect of inactivating OFC projection to V1 during No-Go trials. n = 9 and 13 for EGFP- and Jaws-expressing mice, respectively. For discriminability: $F_{(1, 20)} = 10.24$, $^{**}P = 0.004$. For hit rate: $F_{(1, 20)} = 13.38$, $^{**}P = 0.002$. For CR rate: $F_{(1, 20)} = 6.69$, $^{*}P = 0.02$. Two-way ANOVA with mixed design. **e–g**, Laser stimulation was applied during Go trials. **e**, Similar to those described in **b** except that laser stimulation was applied during Go trials. n = 12 mice in which AAV-CaMKIIα-Jaws-GFP was injected in the OFC. Discriminability: $F_{(1, 11)} = 48.58$, $P = 2.36\times10^{-5}$; hit rate: $F_{(1, 11)} = 2.13$, $P = 0.17$; CR rate: $F_{(1, 11)} = 47.96$, $P = 2.5\times10^{-5}$. Two-way repeated measures ANOVA. **f**, Similar to

those described in **c** except that laser stimulation was applied during Go trials. $n = 11$ mice in which AAV-CaMKIIα-EGFP was injected in the OFC. Discriminability: $F_{(1, 10)} = 38.26$, $P = 1.0\times10^{-4}$; hit rate: $F_{(1, 10)} = 1.6$, $P = 0.23$; CR rate: $F_{(1, 10)} = 44.45$, $P = 5.59\times10^{-5}$. Two-way repeated measures ANOVA. Note that for both control group (**f**) and experimental group (**e**) of mice, laser stimulation during Go trials slightly but significantly increased the discriminability and CR rate of the mice. This may be due to the possibility that laser stimulation served as a cue to guide the mice's behavior. **g**, Effect of inactivating OFC projection to V1 during Go trials. $n = 11$ and 12 for EGFP- and Jaws-expressing mice, respectively. For discriminability: $F_{(1, 21)} = 0.13$, $P = 0.72$. For hit rate: $F_{(1, 21)} = 0.24$, $P = 0.63$. For CR rate: $F_{(1, 21)} = 0.13$, $P = 0.72$. Error bars, mean ± s.e.m.

However, compared to the EGFP-expressing control mice (Fig. 6c), laser stimulation during No-Go trials slowed the learning in Jaws-expressing mice (Fig. 6d). For the experiments that laser stimulation was applied during Go trials, the performance was higher in laser-on than in laser-off trials for both the control and Jaws-expressing mice (Fig. 6e, f), which may be due to the possibility that laser stimulation served as a cue to guide the mice's behavior. Nevertheless, the Jaws-expressing and control mice did not differ in their learning curves when laser stimulation was applied during Go trials (Fig. 6g), indicating that inactivating OFC axons in V1 during Go trials had no effect on the learning process. Together, the results demonstrate that learning to correctly reject the reward-irrelevant No-Go stimulus requires the activity of OFC projection to V1.

We further examined whether the learning process could be affected by optogenetic activation of the OFC top-down projection (Fig. 7a). We found that activation of OFC axons in V1 during No-Go or Go trials both caused an increase in

457 the CR rate in the session with laser stimulation, but the effect disappeared in the next
458 session without laser stimulation (Fig. 7b, c). Such transient effect was likely due to
459 antidromic activation of the OFC neurons (Fig. 1g) that may activate other neurons or
460 pathways involved in performing the task. Given that SST interneurons in V1 were
461 innervated by OFC axons (Supplementary Fig. 2) and were the predominant
462 interneuron subtype showing activity elevation following photostimulation of OFC
463 neurons *in vivo* (Fig. 2i, j), we next examined whether activating SST interneurons in
464 V1 could affect the learning process. This experiment was carried out using SST-Cre
465 mice in which AAVs encoding Cre-dependent ChrimsonR or tdTomato alone were
466 injected into V1 (Fig. 7d). In each session of the learning process, laser stimulation of
467 V1 was applied during No-Go trials, and blocks of laser-on and laser-off trials were
468 interleaved. We found that activating SST interneurons in V1 during No-Go trials did
469 not affect immediate performance in each session, as shown by similar d' and CR rate
470 between laser-on and laser-off trials (Fig. 7e). However, the d' and CR rate of
471 ChrimsonR-expressing mice were significantly higher than those of control mice
472 expressing tdTomato only (Fig. 7f, g). After multiple sessions with laser stimulation
473 during No-Go trials, the higher d' and CR rate in ChrimsonR-expressing mice
474 persisted on later sessions where laser stimulation was no longer applied (Fig. 7g),
475 indicating that the improved performance was indeed due to learning. Thus, SST
476 interneurons in V1 play an important role in the learning of correct rejection for the
477 No-Go stimulus, serving as a substrate for modulating visual associative learning by

the OFC to V1 pathway.

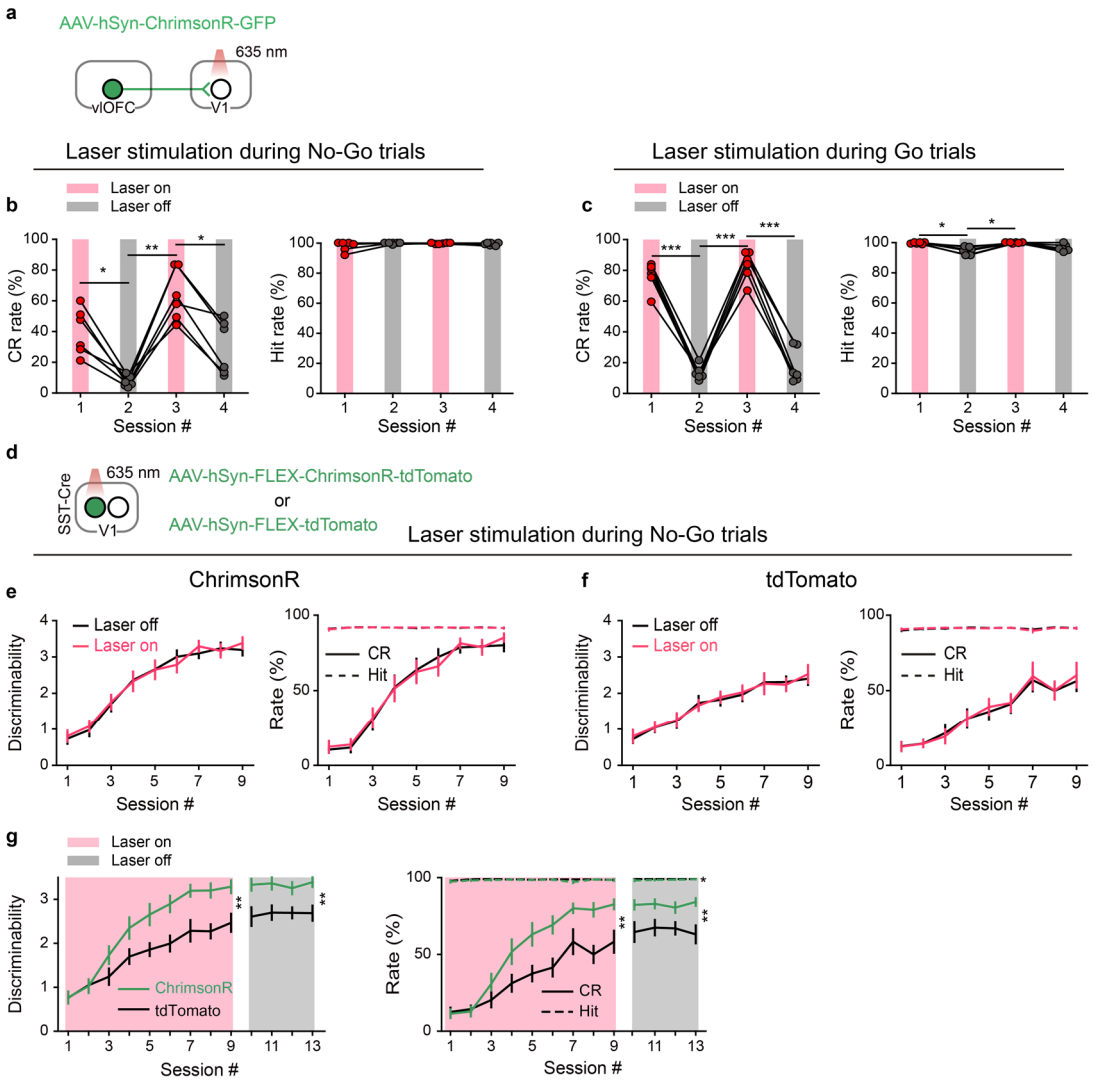

Fig. 7 | Effect of activating OFC projection to V1 or activating SST interneurons in V1 on the performance of Go/No-Go visual task. a, Schematic of viral strategy to achieve optogenetic activation of OFC axons in V1. **b**, Behavioral performance of 6 mice (C57BL/6) in which laser stimulation of V1 was applied during No-Go trials in the first and third sessions. Left, CR rate. $*P < 0.05$, $**P < 0.01$, one-way repeated measures ANOVA with the Greenhouse-Geisser correction ($F_{(1.94, 9.70)} = 33.11$, $P = 4.96\times10^{-5}$) followed by Sidak's multiple comparisons test. Right, hit rate. $F_{(1.15, 5.75)} = 1.81$, $P = 0.23$, one-way repeated measures ANOVA. **c**, Behavioral performance of another group of 6 mice (C57BL/6) in which laser stimulation of V1 was applied during Go trials in the first and third sessions. Left, CR rate. $***P < 0.001$, one-way repeated measures ANOVA with the Greenhouse-Geisser correction ($F_{(1.99, 9.96)} = 161.93$, $P = 2.57\times10^{-8}$) followed by Sidak's multiple comparisons test. Right, hit rate. $*P < 0.05$, one-way repeated measures ANOVA with the Greenhouse-Geisser correction ($F_{(1.62, 8.09)} = 13.18$, $P = 0.004$) followed by Sidak's multiple comparisons

test. **d**, Schematic of the strategy for activating SST interneurons in V1. **e**–**g**, Laser stimulation was applied during No-Go trials. **e**, Discriminability, hit and CR rates with and without laser stimulation during No-Go trials for SST-Cre mice in which AAV-hSyn-FLEX-ChrimsonR-tdTomato was injected in V1 (n = 11). Discriminability: $F_{(1, 10)}$ = 0.64, P = 0.44; hit rate: $F_{(1,10)}$ = 0.05, P = 0.82; CR rate: $F_{(1, 10)}$ = 0.32, P = 0.59. Two-way repeated measures ANOVA. **f**, Similar to those described in **e** except that AAV-hSyn-FLEX-tdTomato was injected in V1 of SST-Cre mice (n = 10). Discriminability: $F_{(1, 9)}$ = 0.33, P = 0.58; hit rate: $F_{(1, 9)}$ = 0.08, P = 0.78; CR rate: $F_{(1, 9)}$ = 0.76, P = 0.41. Two-way repeated measures ANOVA. **g**, Effect of activating SST interneurons in V1 during No-Go trials. n = 10 and 11 for tdTomato- and ChrimsonR-expressing mice, respectively. Sessions 1–9, with laser stimulation; sessions 10–13, without laser stimulation. For discriminability in sessions 1–9: $F_{(1, 19)}$ = 10.44, $^{**}P$ = 0.004; discriminability in sessions 10–13: $F_{(1, 19)}$ = 11.93, $^{**}P$ = 0.003. For hit rate in sessions 1–9: $F_{(1, 19)}$ = 4.37, P = 0.05; hit rate in sessions 10–13: $F_{(1, 19)}$ = 6.07, $^{*}P$ = 0.02. For CR rate in sessions 1–9: $F_{(1, 19)}$ = 10.63, $^{**}P$ = 0.004; CR rate in sessions 10–13: $F_{(1, 19)}$ = 9.84, $^{**}P$ = 0.005. Error bars, mean ± s.e.m.

Discussion

In this study, we demonstrated that activation of OFC terminals in V1 caused reduction of visual responses in V1 neurons by preferentially recruiting SST interneurons in the local circuit. In mice performing a Go/No-Go visual task, the activity of OFC projection to V1 played an essential role in suppressing V1 responses to the reward-irrelevant No-Go stimulus. Phototagging experiments showed that the responses of V1-projecting OFC neurons to the No-Go stimulus were decreased when the mice incorrectly expected reward. Importantly, we revealed that the OFC projection to V1 is critical for the learning of correctly rejecting the No-Go stimulus.

Top down projections to primary sensory areas play an important role in sensory processing and sensory-guided behavior[42,56]. Activating the projections from cingulate region of the frontal cortex to V1 enhances and suppresses V1 responses for the sites

near and surround axonal activation, respectively[43], consistent with the effect of top-down modulation in selective attention[41]. Top-down projections from the anterior cingulate cortex to V1 carried stimulus prediction, which could be used to compute deviations from expectations and guide learning[46]. Associative learning also enhances the effect of top-down inputs from the retrosplenial cortex in modulating V1 responses[49]. However, few studies have recorded from behaving animals the responses of higher cortical neurons that provide top-down projections to V1[57], and examined the causal role of top-down inputs to V1 in learning[58].

The CTB and virus retrograde tracing in our study showed that, the OFC neurons sending projections to V1 were in the ventrolateral OFC. The V1-projecting OFC neurons target all three subtypes of inhibitory interneurons in V1, similar to that found for OFC projections to auditory cortex[44] and cingulate cortex projections to V1[43]. We found that optogenetic stimulation of OFC neurons *in vivo* preferentially activated SST interneurons in V1, likely due to the inhibition of PV and VIP interneurons by SST interneurons[51]. As optogenetic inactivation of OFC projection to V1 did not affect V1 responses in passive-viewing mice, OFC top-down modulation of V1 responses may be task dependent. Many studies showed that the OFC neurons increased firing in anticipation of reward[2], while some studies also found that a fraction of OFC neurons decreased firing to reward-predicting cues[32,37,59]. In our study, those OFC neurons not identified as V1-projecting showed higher firing rates to the No-Go stimulus when mice incorrectly expected reward (Supplementary Fig. 6l).

544 By contrast, the V1-projecting OFC neurons exhibited response decrease when the
545 mouse expected reward for the Go stimulus in hit trials or for the No-Go stimulus in
546 FA trials. The responses of V1-projecting OFC neurons to the No-Go stimulus were
547 higher during correct than during incorrect expectation, which may cause stronger
548 activation of SST interneurons in V1 during correct expectation, leading to lower V1
549 responses to the No-Go stimulus in CR than in FA trials. For the Go stimulus in hit
550 trials, the V1-projecting OFC neurons reduced responses as compared to the baseline
551 responses. This may account for the observation that inactivating OFC axons in V1
552 during Go trials did not affect the responses of V1 neurons to the Go stimulus. We
553 also found that activating SST interneurons in V1 during No-Go trials facilitated the
554 learning of Go/No-Go task. Overall, our results are in line with recent reports that the
555 activity of SST interneurons during learning may reflect the signals from long-range
556 inputs[49,60].

557 Studies using behavioral paradigms such as outcome devaluation and Pavlovian
558 over-expectation have revealed that the OFC is necessary for using expectations of
559 specific outcome to guide behavior and learning[3,61]. The outcome predictions signaled
560 by the OFC neurons could be utilized by downstream regions such as ventral
561 striatum[62,63], dorsal striatum[62,64], BLA[65,66] and VTA[25,34,67]. OFC lesion or inactivation
562 disrupted the prediction errors signaled by dopaminergic neurons[34,67] and expected
563 reward values by putative non-dopaminergic neurons[67] in VTA. While optogenetic
564 inhibition of VTA-projecting OFC neurons did not impair the acquisition of Pavlovian

565 trace conditioning, it impaired extinction learning and memory[32]. In addition, distinct
566 OFC circuits were found to mediate different aspects of reinforcement learning in
567 value-based decision making[68]. We found that the OFC projection to V1 contributed
568 to the suppression of V1 responses to the reward-irrelevant No-Go stimulus in
569 behaving mice, and optogenetic inactivation of OFC axons in V1 during No-Go trials
570 slowed the learning process. As optogenetic inactivation of OFC projection to V1 did
571 not affect the immediate performance of mice, the impairment in learning may be due
572 to an accumulated effect of V1 response modification, which may in turn contribute to
573 the update of outcome expectation signal in the OFC via the inputs from visual
574 cortex[38-40]. Because the OFC projects to other sensory cortices in addition to V1[38], the
575 OFC top-down projections may also play an important role in associative learning for
576 other sensory modalities.
577

578 **Acknowledgments**

579 We thank M. M. Poo for comments on the manuscript. We thank Y. Li and W. Xu for
580 technical assistance and Y.-N. Dou for help with slice recordings. This work was
581 supported by the Strategic Priority Research Program of Chinese Academy of
582 Sciences (grant No. XDB32010200), Shanghai Municipal Science and Technology
583 Major Project (grant No. 2018SHZDZX05), and the National Natural Science
584 Foundation of China (31571079, 31771151).
585

Author contributions

D.L. and H.Y. conceived and designed the experiments. D.L. performed and organized all the experiments. J.D. and Y.-G.S. performed whole-cell recording experiments. D.L., Z.-Y. Z., H.Y., Z. Z., and T.Y. analyzed the data. H.Y. wrote the manuscript with inputs from all authors. All authors read and revised the manuscript.

Competing interests

The authors declare no competing interests.

References

1 Murray, E. A., O'Doherty, J. P. & Schoenbaum, G. What we know and do not know about the functions of the orbitofrontal cortex after 20 years of cross-species studies. *J. Neurosci.* **27**, 8166-8169 (2007).

2 Schoenbaum, G., Roesch, M. R., Stalnaker, T. A. & Takahashi, Y. K. A new perspective on the role of the orbitofrontal cortex in adaptive behaviour. *Nature Rev. Neurosci.* **10**, 885-892 (2009).

3 Rudebeck, P. H. & Murray, E. A. The orbitofrontal oracle: cortical mechanisms for the prediction and evaluation of specific behavioral outcomes. *Neuron* **84**, 1143-1156 (2014).

4 Thorpe, S. J., Rolls, E. T. & Maddison, S. The orbitofrontal cortex: neuronal activity in the behaving monkey. *Exp. Brain Res.* **49**, 93-115 (1983).

5 Schoenbaum, G. & Eichenbaum, H. Information coding in the rodent prefrontal cortex. I. Single-neuron activity in orbitofrontal cortex compared with that in pyriform cortex. *J. Neurophysiol.* **74**, 733-750 (1995).

6 Schoenbaum, G., Chiba, A. A. & Gallagher, M. Orbitofrontal cortex and basolateral amygdala encode expected outcomes during learning. *Nat. Neurosci.* **1**, 155-159 (1998).

7 Tremblay, L. & Schultz, W. Relative reward preference in primate orbitofrontal cortex. *Nature* **398**, 704-708 (1999).

8 Tremblay, L. & Schultz, W. Modifications of reward expectation-related neuronal activity during learning in primate orbitofrontal cortex. *J.*

Neurophysiol. **83**, 1877-1885 (2000).

9 Hikosaka, K. & Watanabe, M. Delay activity of orbital and lateral prefrontal neurons of the monkey varying with different rewards. *Cereb. Cortex* **10**, 263-271 (2000).

10 Wallis, J. D. & Miller, E. K. Neuronal activity in primate dorsolateral and orbital prefrontal cortex during performance of a reward preference task. *Eur. J. Neurosci.* **18**, 2069-2081 (2003).

11 Roesch, M. R. & Olson, C. R. Neuronal activity related to reward value and motivation in primate frontal cortex. *Science* **304**, 307-310 (2004).

12 Kennerley, S. W. & Wallis, J. D. Evaluating choices by single neurons in the frontal lobe: outcome value encoded across multiple decision variables. *Eur. J. Neurosci.* **29**, 2061-2073 (2009).

13 Kepecs, A., Uchida, N., Zariwala, H. A. & Mainen, Z. F. Neural correlates, computation and behavioural impact of decision confidence. *Nature* **455**, 227-231 (2008).

14 Padoa-Schioppa, C. & Assad, J. A. Neurons in the orbitofrontal cortex encode economic value. *Nature* **441**, 223-226 (2006).

15 Gallagher, M., McMahan, R. W. & Schoenbaum, G. Orbitofrontal cortex and representation of incentive value in associative learning. *J. Neurosci.* **19**, 6610-6614 (1999).

16 Pickens, C. L. *et al.* Different roles for orbitofrontal cortex and basolateral amygdala in a reinforcer devaluation task. *J. Neurosci.* **23**, 11078-11084 (2003).

17 Pickens, C. L., Saddoris, M. P., Gallagher, M. & Holland, P. C. Orbitofrontal lesions impair use of cue-outcome associations in a devaluation task. *Behav. Neurosci.* **119**, 317-322 (2005).

18 Schoenbaum, G., Setlow, B., Nugent, S. L., Saddoris, M. P. & Gallagher, M. Lesions of orbitofrontal cortex and basolateral amygdala complex disrupt acquisition of odor-guided discriminations and reversals. *Learn Mem* **10**, 129-140 (2003).

19 Izquierdo, A., Suda, R. K. & Murray, E. A. Bilateral orbital prefrontal cortex lesions in rhesus monkeys disrupt choices guided by both reward value and reward contingency. *J. Neurosci.* **24**, 7540-7548 (2004).

20 McDannald, M. A., Saddoris, M. P., Gallagher, M. & Holland, P. C. Lesions of orbitofrontal cortex impair rats' differential outcome expectancy learning but not conditioned stimulus-potentiated feeding. *J. Neurosci.* **25**, 4626-4632 (2005).

21 Machado, C. J. & Bachevalier, J. The effects of selective amygdala, orbital frontal cortex or hippocampal formation lesions on reward assessment in nonhuman primates. *Eur. J. Neurosci.* **25**, 2885-2904 (2007).

22 West, E. A., DesJardin, J. T., Gale, K. & Malkova, L. Transient inactivation of orbitofrontal cortex blocks reinforcer devaluation in macaques. *J. Neurosci.* **31**,

15128-15135 (2011).

23 Rudebeck, P. H. & Murray, E. A. Dissociable effects of subtotal lesions within the macaque orbital prefrontal cortex on reward-guided behavior. *J. Neurosci.* **31**, 10569-10578 (2011).

24 Burke, K. A., Franz, T. M., Miller, D. N. & Schoenbaum, G. The role of the orbitofrontal cortex in the pursuit of happiness and more specific rewards. *Nature* **454**, 340-344 (2008).

25 Takahashi, Y. K. *et al.* The orbitofrontal cortex and ventral tegmental area are necessary for learning from unexpected outcomes. *Neuron* **62**, 269-280 (2009).

26 McDannald, M. A., Lucantonio, F., Burke, K. A., Niv, Y. & Schoenbaum, G. Ventral striatum and orbitofrontal cortex are both required for model-based, but not model-free, reinforcement learning. *J. Neurosci.* **31**, 2700-2705 (2011).

27 Ostlund, S. B. & Balleine, B. W. Orbitofrontal cortex mediates outcome encoding in Pavlovian but not instrumental conditioning. *J. Neurosci.* **27**, 4819-4825 (2007).

28 Jones, J. L. *et al.* Orbitofrontal cortex supports behavior and learning using inferred but not cached values. *Science* **338**, 953-956 (2012).

29 Gremel, C. M. & Costa, R. M. Premotor cortex is critical for goal-directed actions. *Front Comput Neurosci* **7**, 110 (2013).

30 Gardner, M. P. H., Conroy, J. S., Shaham, M. H., Styer, C. V. & Schoenbaum, G. Lateral Orbitofrontal Inactivation Dissociates Devaluation-Sensitive Behavior and Economic Choice. *Neuron* **96**, 1192-1203 e1194 (2017).

31 Rudebeck, P. H., Saunders, R. C., Prescott, A. T., Chau, L. S. & Murray, E. A. Prefrontal mechanisms of behavioral flexibility, emotion regulation and value updating. *Nat. Neurosci.* **16**, 1140-1145 (2013).

32 Namboodiri, V. M. K. *et al.* Single-cell activity tracking reveals that orbitofrontal neurons acquire and maintain a long-term memory to guide behavioral adaptation. *Nat. Neurosci.* **22**, 1110-1121 (2019).

33 Saddoris, M. P., Gallagher, M. & Schoenbaum, G. Rapid associative encoding in basolateral amygdala depends on connections with orbitofrontal cortex. *Neuron* **46**, 321-331 (2005).

34 Takahashi, Y. K. *et al.* Expectancy-related changes in firing of dopamine neurons depend on orbitofrontal cortex. *Nat. Neurosci.* **14**, 1590-1597 (2011).

35 Schultz, W. & Dickinson, A. Neuronal coding of prediction errors. *Annu. Rev. Neurosci.* **23**, 473-500 (2000).

36 Niv, Y. & Schoenbaum, G. Dialogues on prediction errors. *Trends Cogn. Sci.* **12**, 265-272 (2008).

37 Takahashi, Y. K. *et al.* Neural estimates of imagined outcomes in the orbitofrontal cortex drive behavior and learning. *Neuron* **80**, 507-518 (2013).

38 Zingg, B. *et al.* Neural networks of the mouse neocortex. *Cell* **156**, 1096-1111 (2014).

39 Cavada, C., Company, T., Tejedor, J., Cruz-Rizzolo, R. J. & Reinoso-Suarez, F. The anatomical connections of the macaque monkey orbitofrontal cortex. A review. *Cereb. Cortex* **10**, 220-242 (2000).

40 Carmichael, S. T. & Price, J. L. Sensory and premotor connections of the orbital and medial prefrontal cortex of macaque monkeys. *J. Comp. Neurol.* **363**, 642-664 (1995).

41 Moore, T. & Armstrong, K. M. Selective gating of visual signals by microstimulation of frontal cortex. *Nature* **421**, 370-373 (2003).

42 Gilbert, C. D. & Li, W. Top-down influences on visual processing. *Nature Rev. Neurosci.* **14**, 350-363 (2013).

43 Zhang, S. *et al.* Selective attention. Long-range and local circuits for top-down modulation of visual cortex processing. *Science* **345**, 660-665 (2014).

44 Winkowski, D. E. *et al.* Orbitofrontal Cortex Neurons Respond to Sound and Activate Primary Auditory Cortex Neurons. *Cereb. Cortex* (2017).

45 Manita, S. *et al.* A Top-Down Cortical Circuit for Accurate Sensory Perception. *Neuron* **86**, 1304-1316 (2015).

46 Fiser, A. *et al.* Experience-dependent spatial expectations in mouse visual cortex. *Nat. Neurosci.* **19**, 1658-1664 (2016).

47 Leinweber, M., Ward, D. R., Sobczak, J. M., Attinger, A. & Keller, G. B. A sensorimotor circuit in mouse cortex for visual flow predictions. *Neuron* **95**, 1420-1432 e1425 (2017).

48 Poort, J. *et al.* Learning enhances sensory and multiple non-sensory representations in primary visual cortex. *Neuron* **86**, 1478-1490 (2015).

49 Makino, H. & Komiyama, T. Learning enhances the relative impact of top-down processing in the visual cortex. *Nat. Neurosci.* **18**, 1116-1122 (2015).

50 Wall, N. R., Wickersham, I. R., Cetin, A., De La Parra, M. & Callaway, E. M. Monosynaptic circuit tracing in vivo through Cre-dependent targeting and complementation of modified rabies virus. *Proc. Natl. Acad. Sci. USA.* **107**, 21848-21853 (2010).

51 Pfeffer, C. K., Xue, M., He, M., Huang, Z. J. & Scanziani, M. Inhibition of inhibition in visual cortex: the logic of connections between molecularly distinct interneurons. *Nat. Neurosci.* **16**, 1068-1076 (2013).

52 Carrillo-Reid, L., Han, S., Yang, W., Akrouh, A. & Yuste, R. Controlling Visually Guided Behavior by Holographic Recalling of Cortical Ensembles. *Cell* **178**, 447-457 e445 (2019).

53 Stringer, C. *et al.* Spontaneous behaviors drive multidimensional, brainwide activity. *Science* **364**, 255 (2019).

54 Tervo, D. G. *et al.* A designer AAV variant permits efficient retrograde access to projection neurons. *Neuron* **92**, 372-382 (2016).

55 Kvitsiani, D. *et al.* Distinct behavioural and network correlates of two interneuron types in prefrontal cortex. *Nature* **498**, 363-366 (2013).

56 Makino, H., Hwang, E. J., Hedrick, N. G. & Komiyama, T. Circuit Mechanisms of Sensorimotor Learning. *Neuron* **92**, 705-721 (2016).

57 Vélez-Fort, M. *et al.* A Circuit for Integration of Head- and Visual-Motion Signals in Layer 6 of Mouse Primary Visual Cortex. *Neuron* **98**, 179-191 e176 (2018).

58 Chubykin, A. A., Roach, E. B., Bear, M. F. & Shuler, M. G. A cholinergic mechanism for reward timing within primary visual cortex. *Neuron* **77**, 723-735 (2013).

59 Zhou, J., Jia, C., Feng, Q., Bao, J. & Luo, M. Prospective coding of dorsal raphe reward signals by the orbitofrontal cortex. *J. Neurosci.* **35**, 2717-2730 (2015).

60 Khan, A. G. *et al.* Distinct learning-induced changes in stimulus selectivity and interactions of GABAergic interneuron classes in visual cortex. *Nat. Neurosci.* **21**, 851-859 (2018).

61 McDannald, M. A., Jones, J. L., Takahashi, Y. K. & Schoenbaum, G. Learning theory: a driving force in understanding orbitofrontal function. *Neurobiol. Learn. Mem.* **108**, 22-27 (2014).

62 Berendse, H. W., Galis-de Graaf, Y. & Groenewegen, H. J. Topographical organization and relationship with ventral striatal compartments of prefrontal corticostriatal projections in the rat. *J. Comp. Neurol.* **316**, 314-347 (1992).

63 Cooch, N. K. *et al.* Orbitofrontal lesions eliminate signalling of biological significance in cue-responsive ventral striatal neurons. *Nat. Commun.* **6**, 7195 (2015).

64 Pascoli, V. *et al.* Stochastic synaptic plasticity underlying compulsion in a model of addiction. *Nature* **564**, 366-371 (2018).

65 Sharpe, M. J. & Schoenbaum, G. Back to basics: Making predictions in the orbitofrontal-amygdala circuit. *Neurobiol. Learn. Mem.* **131**, 201-206 (2016).

66 Murray, E. A. & Wise, S. P. Interactions between orbital prefrontal cortex and amygdala: advanced cognition, learned responses and instinctive behaviors. *Curr. Opin. Neurobiol.* **20**, 212-220 (2010).

67 Jo, Y. S. & Mizumori, S. J. Y. Prefrontal Regulation of Neuronal Activity in the Ventral Tegmental Area. *Cereb. Cortex* **26**, 4057-4068 (2016).

68 Groman, S. M. *et al.* Orbitofrontal Circuits Control Multiple Reinforcement-Learning Processes. *Neuron* **103**, 734-746 e733 (2019).

Methods

Animals. All animal procedures were approved by the Animal Care and Use Committee at the Institute of Neuroscience, Chinese Academy of Sciences, and were in accordance with the guidelines of the Animal Advisory Committee at the Shanghai

778 Institutes for Biological Sciences.

779 We used the following mice: GAD67-GFP (CB6-Tg(Gad1-EGFP)G42Zjh),
780 CaMKIIα-Cre (B6.Cg-Tg(Camk2a-cre)T29-1Stl), SST-Cre ($Sst^{tm2.1(cre)Zjh}$), PV-Cre
781 (B6;129P2-$Pvalb^{tm1(cre)Arbr}$), VIP-Cre ($Vip^{tm1(cre)Zjh}$), SST::Ai9 (generated by crossing
782 SST-Cre with Ai9 mice, B6.Cg-Gt(ROSA)26$Sor^{tm9(CAG-tdTomato)Hze}$), PV::Ai9, VIP::Ai9
783 and C57BL/6 mice. Adult (2 – 4 months) male mice were used for all experiments.
784
785 **Adeno-Associated Virus (AAVs).** We used the following AAVs: rAAV2-retro-hSyn-
786 Cre (titer: 3.2 $\times 10^{12}$ viral particles/ml) and AAV2/8-EF1a-DIO-EYFP-WPRE (titer:
787 6.9×10^{12} viral particles/ml, for visualizing OFC axons in V1 in Fig. 1b); AAV2/8-
788 CaMKIIα-hChR2(H134R)-mCherry (titer: 8.26×10^{12} viral particles/ml) and AAV2/8-
789 hSyn-ChrimsonR-GFP (titer: 6.58×10^{12} viral particles/ml) (for activating OFC
790 projection to V1 in Fig. 1, Fig. 7 and Supplementary Fig. 1, or for activating OFC in
791 Fig. 2g–k); AAV2/8-CaMKIIα-hChR2(H134R)-EYFP (titer: 8.66×10^{12} viral
792 particles/ml; for activating OFC projection to V1 in Fig. 2a–f); AAV2/9-hSyn-FLEX-
793 GCaMP6s-WPRE (titer: 6.9×10^{12} viral particles/ml; for fiber photometry experiment
794 in Fig. 2g–k); AAV2/9-EF1α-DIO-His-EGFP-2A-TVA-WPRE (titer: 1.26×10^{12} viral
795 particles/ml), AAV2/9-EF1α-DIO-RVG-WPRE (titer: 3.12×10^{12} viral particles/ml)
796 and RV-EnvA-ΔG-dsRed (titer: 1×10^{8} viral particles/ml)(for retrograde monosynaptic
797 tracing in Supplementary Fig. 2); AAV2/8-hSyn-Jaws-KGC-GFP-ER2 (titer: 5.4×10^{12}
798 viral particles/ml; for inactivating OFC projection to V1 in Fig. 4, Supplementary Fig.

799 1, Supplementary Fig. 4 and Supplementary Fig. 5); rAAV2-retro-hSyn-ChrimsonR-
800 GFP (titer: 5.63×10^{12} viral particles/ml; for optogenetic tagging of V1-projecting OFC
801 neurons in Fig. 5 and Supplementary Fig. 6); AAV2/8-CaMKIIα-Jaws-KGC-GFP-
802 ER2 (titer: 5.38×10^{12} viral particles/ml; for inactivating OFC projection to V1 in Fig.
803 6); AAV2/8-hSyn-FLEX-ChrimsonR-tdTomato (titer: 3.7×10^{12} viral particles/ml; for
804 activating SST interneurons in Fig. 7); AAV2/8-CaMKIIα-EGFP-WPRE (titer:
805 5.8×10^{12} viral particles/ml), AAV2/8-CaMKIIα-mCherry (titer: 5.7×10^{12} viral
806 particles/ml), AAV2/8-hSyn-FLEX-tdTomato (titer: 5.1×10^{12} viral particles/ml) and
807 AAV-hSyn-EGFP-WPRE (titer: 7.3×10^{12} viral particles/ml) (for optogenetic or fiber
808 photometry experiments as a control group in Fig. 2i, Fig. 6, Supplementary Fig. 1,
809 and Supplementary Fig. 4).
810
811 **Surgery.** The mice were anesthetized with a mixture of midazolam (5 mg/kg),
812 fentanyl (0.05 mg/kg) and medetomidine (0.5 mg/kg), and were head-fixed in a
813 stereotaxic apparatus. For behavioral experiments without optogenetic manipulation,
814 head plates were implanted before behavioral training. For *in vivo* recording and
815 behavioral experiments with optogenetic manipulation, head plates were implanted
816 after the virus injection. The virus was injected with a glass pipette (10 – 20 μm tip
817 diameter) using a syringe pump (Harvard Apparatus). To observe the OFC axons in
818 V1, we injected rAAV2-retro-hSyn-Cre (100 nl) in V1 (AP, -3.5 mm; ML, 2.4 mm;
819 DV, 0.5 mm) and AAV2/8-EF1a-DIO-EYFP-WPRE (500 nl) in the OFC (AP, 2.7 mm;

820 ML, 0.88 mm; DV, 1.8 mm). To manipulate the OFC to V1 projection in C57BL/6
821 mice, a craniotomy was made above the right OFC (AP, 2.7 mm; ML, 0.88 mm), and
822 500 nl of AAV (AAV2/8-hSyn-Jaws-KGC-GFP-ER2, AAV2/8-CaMKIIα-Jaws-KGC-
823 GFP-ER2, AAV2/8-CaMKIIα-hChR2(H134R)-mCherry, AAV2/8-CaMKIIα-
824 hChR2(H134R)-EYFP, AAV2/8-hSyn-ChrimsonR-GFP; or the control virus: AAV2/8-
825 CaMKIIα-EGFP-WPRE or AAV2/8-CaMKIIα-mCherry) were injected into the cortex
826 at a depth of 1.8 mm. A rectangular region on the skull above V1 (AP, -3.2 to -3.8
827 mm; ML, 2.0 to 2.8 mm) ipsilateral to the OFC injection site was marked by cutting
828 and permanent red ink. The marked skull region above V1 was covered with tissue
829 glue (Vetbond, 3M) until optogenetic manipulation or *in vivo* recording. For the
830 experiments to block antidromic spiking of OFC neurons caused by laser stimulation
831 of OFC axons in V1, a cannula (0.41 mm diameter) was implanted 500 μm above the
832 virus injection site in the OFC. For fiber photometry recording, AAV2/8-CaMKIIα-
833 hChR2(H134R)-mCherry (600 nl) was injected to the right OFC at a depth of 1.8 mm
834 and AAV2/9-hSyn-FLEX-GCaMP6s-WPRE (300 nl) was injected to the right V1 at a
835 depth of 0.5 mm in SST-Cre, PV-Cre or VIP-Cre mice. Following the virus injection,
836 one optical fiber (200 μm diameter, NA 0.37) was inserted 100 μm above the injection
837 site in the OFC and another one touching the dura of injection site in V1. For
838 phototagging of V1-projecting OFC neurons, a craniotomy was made above the right
839 V1 (AP, -3.5 mm; ML, 2.4 mm), and rAAV2-retro-hSyn-ChrimsonR-GFP (300 nl)
840 were injected into the cortex at a depth of 0.5 mm. To activate SST interneurons in V1

841 of SST-Cre mice, AAV2/8-hSyn-FLEX-ChrimsonR-tdTomato (300 nl) were injected
842 into V1 at a depth of 0.5 mm, and the craniotomy was protected with a silicone
843 elastomer (Kwik-Sil, WPI). After the virus injection, a stainless-steel headplate was
844 fixed to the skull using dental cement. For mice used for Go/No-Go behavior with
845 optogenetic manipulation of OFC axons in V1 or SST interneurons in V1, dental
846 cement mixed with 50% carbon powder was used to cover the skull except the region
847 above V1. The mice were injected with carprofen (5 mg/kg) subcutaneously after the
848 surgery for 3 days, and were allowed to recover with food and water *ad libitum* for at
849 least 7 days.

850 For infusion of tetrodotoxin (TTX) in the OFC, 1 μl of TTX (4 μM) was injected
851 into the OFC through the implanted cannula 0.5 – 1 h before the *in vivo* recording.

852 Fluorescently conjugated Cholera toxin subunit B (CTB-555, 2 μg/μl, 300 nl,
853 Invitrogen) was injected unilaterally into V1 (AP, -3.5 mm; ML, 2.4 mm) in C57BL/6
854 or GAD67-GFP mice. In some C57BL/6 mice, both CTB and rAAV2-retro-hSyn-
855 ChrimsonR-GFP were injected in V1 to estimate the percentage of OFC neurons co-
856 labeled by GFP and CTB. The histology experiments were performed 2 weeks after
857 the injection.

858 Glycoprotein-deleted (ΔG) and EnvA-pseudotyped rabies virus (RV-EnvA-ΔG-
859 dsRed) was used for retrograde monosynaptic tracing from different types of V1
860 neurons[50]. TVA receptor and rabies glycoprotein were expressed in Cre-positive
861 neurons by co-injection of AAV2/9-EF1α-DIO-His-EGFP-2A-TVA-WPRE and

AAV2/9-EF1α-DIO-RVG-WPRE (300 nl) in V1 in CaMKIIα-Cre, PV-Cre, SST-Cre and VIP-Cre mice. RV-EnvA-ΔG-dsRed (300 nl) was injected in the same site two weeks later. The histology experiments were performed 8 d after the RV injection.

***In vivo* extracellular recording.** Recordings with optogenetic stimulation were performed at least 3 weeks after the virus injection. For anesthetized experiments, mice were injected with chlorprothixene (3.2 mg/kg) subcutaneously and anesthetized with urethane (0.7 – 1.0 g/kg) intraperitoneally. The mouse was head-fixed in a stereotaxic frame and its body temperature was maintained at 37 ℃ through a heating blanket (FHC Inc.). A craniotomy (~ 1 mm diameter) was made above V1 (AP, -3.5 mm; ML, 2.4 mm). For recordings in awake mice, the body of the mouse was restricted in a circular plastic tube and the headplate was fixed to a holder attached to the stereotaxic apparatus. While the animal was anesthetized with isoflurane (1 – 2%), a craniotomy (~ 1 mm diameter) was made above V1 (AP, -3.5 mm; ML, 2.4 mm) or OFC (AP, 2.7 mm; ML 0.88 mm). The dura was removed, and the craniotomy was covered by ~1% agarose dissolved in artificial cerebral spinal fluid (ACSF) and protected by a silicone elastomer (Kwik-Cast, WPI). The mouse was allowed to recover from the anesthesia in home cage for at least 1 hour. The recordings were made with multi-site silicon probes (A1×16-3mm-50-177 or A1×16-5mm-50-177, NeuroNexus Technologies; ASSY-77.2-64-6, Diagnostic Biochips, Inc.) mounted on a manipulator (MP-225, Sutter Instrument Company). For some recordings, the silicon

883 probe was coated with DiO (Invitrogen) to allow *post hoc* recovery of penetration
884 track. After finishing the recordings from awake mice, the electrode was retracted.
885 The craniotomy was cleaned with ACSF, covered with ~1% agarose and protected
886 with a silicone elastomer (Kwik-Cast, WPI). After the experiments, the mouse was
887 euthanized by an overdose of sodium pentobarbital.
888 The neural responses were amplified and filtered using a Cerebus 64-channel
889 system (Blackrock microsystems). Local field potential signals were sampled at 2 kHz
890 with a wide-band front-end filter (0.3 – 500 Hz). Spiking signals were sampled at 30
891 kHz. To detect the waveforms of spikes, we band-pass filtered the signals at 250 –
892 7500 Hz and set a threshold at 3.5 s.d. of the background noise. Spikes were sorted
893 offline using the Offline Sorter (Plexon Inc.) based on cluster analysis of principle
894 component amplitude. Spike clusters were considered to be single units if the
895 percentage of spikes with interspike interval < 1 ms was lower than 0.3% and the *P*
896 value for multivariate analysis of variance tests on clusters was less than 0.05.
897
898 **Slice preparation and recording.** We used C57BL/6, SST::Ai9, PV::Ai9 and
899 VIP::Ai9 mice for slice recordings. Mice that had been injected with AAV2/8-
900 CaMKIIα-hChR2(H134R)-EYFP in the OFC were anesthetized with isoflurane and
901 perfused with ice-cold cutting solution containing the following (in mM): sucrose
902 234, KCl 2.5, NaH_2PO_4 1.25, $MgSO_4$ 10, $CaCl_2$ 0.5, $NaHCO_3$ 26 and glucose 11 (300
903 – 305 mOsm). The mouse brain was dissected, and coronal slices (300 μm) were

prepared using a vibratome (Leica VT1200S) in the ice-cold cutting solution. The prepared brain slices of V1 were incubated in ACSF containing the following (in mM): NaCl 126, KCl 2.5, NaH_2PO_4 1.25, $MgCl_2$ 2, $CaCl_2$ 2, $NaHCO_3$ 26 and glucose 10 (300 – 305 mOsm) for 30 – 45 min at 34°C, and then kept at room temperature. The cutting solution and ACSF were bubbled with 95% O_2 and 5% CO_2.

Whole-cell recordings of V1 neurons in voltage-clamp mode were made at room temperatures (25 – 28°C) with a Multiclamp 700B amplifier and a Digidata 1440A (Molecular Devices). The electrodes were filled with a Cs-based low Cl^- internal solution containing the following (in mM): $CsMeSO_3$ 130, $MgCl_2$ 1, $CaCl_2$ 1, HEPES 10, QX-314 2, EGTA 11, Mg-ATP 2, Na-GTP 0.3 (pH 7.3, 295 mOsm). Excitatory and inhibitory currents were recorded at -70 mV and 0 mV, respectively. Different types of V1 inhibitory neurons were identified by tdTomato-expressing neurons in SST::Ai9, PV::Ai9 and VIP::Ai9 mice. Pyramidal neurons were identified based on the morphology of tdTomato-negative cells and verified by staining of biocytin, which was included in the internal solution. Picrotoxin (50 μM, Tocris) and NBQX (10 μM, Tocris) were used to block $GABA_A$ receptor and AMPA receptor mediated currents, respectively. Data were sampled at 10 or 20 kHz and analyzed with pCLAMP 10 (Molecular Devices).

Fiber photometry. For fluorescence Ca^{2+} recordings, light from a 473-nm LED was reflected by a dichroic mirror (MD498, Thorlabs). The emission signals collected

through the implanted optical fiber in V1 were filtered by a bandpass filter (MF525-39, Thorlabs) and detected by a photomultiplier tube (PMT, R3896, Hamamatsu). The light at the tip of the optical fiber was adjusted to 10 – 30 μW to minimize bleaching. An amplifier converted the output of the PMT to voltage signals, which were digitized using a data acquisition card (USB6009, National Instrument) at 200 Hz with custom-written programs.

Visual stimulation. For *in vivo* recording experiments, visual stimuli were presented on a 17" LCD monitor (Dell P170S, mean luminance of 35 cd/m^2, refresh rate 60 Hz) placed 9 cm away from the eye contralateral to the recording site, subtending 112.6° × 124.2° of visual space. Gamma correction was used to calibrate the monitor. The position of the monitor was adjusted such that the receptive fields (RFs) of the recorded neurons were at the center of the monitor. To locate the RFs of V1 neurons, we presented sparse noise stimuli over a black background, in which a white square (21° × 21°) was flashed for 33.3 ms on a 112.6° square grid in a pseudorandom sequence (100 repeats). To measure orientation tuning with and without inactivating OFC axons in V1, we presented drifting gratings (96° × 96°, spatial frequency = 0.03 cycles/deg, temporal frequency = 2 Hz, contrast = 100%) at 12 different directions (spaced at 30°) in a random sequence. Each stimulus was repeated 14 times for both laser-off and laser-on conditions. Each trial of the stimulus started with 1 s of gray screen, followed by 0.5 s of the first frame of grating and 2 s of the drifting grating.

946 For behavioral experiments, oriented gratings (90° × 90°, spatial frequency = 0.04
947 cycles/deg, contrast = 100%) were presented on a 17" LCD monitor (Dell E1713S,
948 mean luminance 40 cd/m^2, refresh rate 60 Hz) placed ~10 cm away from the eye
949 contralateral to the recording site or virus injection site. The Go and No-Go stimuli
950 were vertically and horizontally oriented gratings, respectively. In each trial, the
951 vertically (horizontally) oriented grating was static during the waiting period and then
952 drifting rightward (upward) during the answer period. The Go and No-Go trials were
953 randomly interleaved.
954
955 **Behavioral task.** Mice were water-deprived for 2 days before the behavioral training.
956 During behavioral experiments, the mouse was head-fixed and sat in an acrylic tube
957 within a training box. Tongue licks were detected by the interruption of an infrared
958 beam or a capacitance touch sensor, and the delivery of water was controlled by a
959 peristaltic valve (Kamoer). The mice went through a habituation phase and a
960 conditioning phase before learning the Go/No-Go task. For habituation (2 days), the
961 mouse learned to lick from a custom-made lickspout to get water reward every 4 s.
962 For conditioning (2 – 3 days), the mouse was trained to lick in response to a vertically
963 oriented grating stimulus. The grating was static for 0.7 s or 0.5 s (waiting period) and
964 then drifting for 2.2 s or 2.4 s (answer period). If a lick was detected during the
965 answer period, the mouse was rewarded with 5.5 μl of water. For Go/No-Go task, the
966 grating stimulus in each trial was static during the waiting period and drifting during

the answer period. For some groups of mice (Fig. 3, Fig. 4, Fig. 5, Supplementary Fig. 3–6), the durations of waiting period and answer period were 0.7 s and 2.2 s, respectively. For other groups of mice (Fig. 6 and Fig. 7), the durations of waiting period and answer period were 0.5 s and 2.4 s, respectively. Licking during the waiting period was neither rewarded nor punished. For a Go stimulus, if a lick was detected during the answer period, the mouse was rewarded with 5.5 μl of water upon lick detection (hit). The mouse was neither rewarded nor punished for a miss (no lick during the answer period of Go stimulus), CR (no lick during the answer period of No-Go stimulus) or FA (lick during the answer period of No-Go stimulus). During the inter-trial interval (ITI), the screen was blank and licking was punished by a timeout period of 4 s. Licking during the 4-s timeout period triggered another 4-s timeout unless no lick was detected during the timeout period or the accumulated timeout exceeded 20 s. Each mouse performed the task for 1 h in each session.

In a subset of behavioral sessions, we recorded images of the facial area ipsilateral to the V1 recording site with a point grey camera (30 Hz frame rate) and a 780 nm longpass filter. Infrared LEDs (840 nm) were used to illuminate the face of the mouse.

Optogenetic stimulation. Optical activation of ChR2 (ChrimsonR) was induced by blue (red) light. Optical silencing by Jaws activation was induced by red light. A blue laser (473 nm) or a red laser (635 nm) (Shanghai Laser & Optics Century Co.) was

988 connected to an output optical fiber and the laser was controlled by a stimulus
989 generator (Master 9, A.M.P.I.).

990 For measuring synaptic inputs from OFC axons to V1 neurons during slice
991 recording experiments, blue light (1 ms duration) was delivered through a 40×0.8 NA
992 water immersion lens at a power of 50 mW.

993 To manipulate the activity of OFC axons in V1 for *in vivo* recording or behavioral
994 experiments, we used a zoom fiber collimator to focus the laser beam (~600 μm
995 diameter) on V1 or on the center of the marked skull region above V1. A shield was
996 mounted on the mouse's head to prevent leakage of laser light to the eyes or to the
997 screen.

998 For *in vivo* extracellular recording of V1 neurons with optogenetic manipulation,
999 trials with and without laser stimulation were interleaved. Laser stimulation covered
1000 the duration of stimulus presentation. For V1 recordings with laser stimulation during
1001 Go trials, the laser was turned on 100-ms before the onset of visual stimulus (Fig.
1002 4a–d). For V1 recordings with laser stimulation during No-Go trials, the laser was
1003 turned on 100-ms before stimulus onset for some mice and at stimulus onset for other
1004 mice (Fig. 4e–l and Supplementary Fig. 4). Laser was at a power of 5 mW at
1005 collimator output for blue laser and 10 mW for red laser.

1006 For behavioral experiments in which the OFC to V1 projection was
1007 optogenetically inactivated or SST interneurons in V1 were activated, laser-off and
1008 laser-on blocks (20 trials/block) were interleaved in each session. In laser-on blocks,

laser stimulation was applied during No-Go trials and Go trials in two separate groups of mice, respectively. During trials with laser stimulation, the laser was turned on 100−ms before stimulus onset, and turned off at stimulus offset. Laser was at a power of 10 or 15 mW at collimator output.

For fiber photometry recording experiments, 100 – 150 pulses of blue laser light (500 ms duration, interval at 10 s) were delivered to the optical fiber implanted in the OFC.

For phototagging of the V1-projecting OFC neurons, red laser light (15 mW) was applied on the surface of cortical area above the OFC ipsilateral to the virus injection site in V1. We delivered 400 light pulses (each 5-ms long) at 0.5 Hz.

Histology. At least two weeks after the tracer/virus injection in V1 or virus injection in the OFC, the mouse was deeply anesthetized with sodium pentobarbital (120 mg/kg) and was perfused with 60 ml saline followed by 60 ml paraformaldehyde (PFA, 4%). Brains were collected, fixed in 4% PFA (4°C) overnight, and then transferred to 30% sucrose in phosphate-buffered saline (PBS) until equilibration. Brain sections (40 μm) were cut using a cryostat (Microm). The floating sections were incubated with Hoechst (2 μM, Thermo Fisher Scientific) in PBS for 10 min. The sections were rinsed in PBS for 10 min, mounted onto glass slides and coverslipped with VECTASHIELD Antifade Mounting Medium (Vector Laboratories, H-1000). Fluorescence images were taken with a Nikon A1 (Nikon Co. Ltd.) confocal

microscope or the VS120 (Olympus). Images were analyzed with ImageJ (NIH, US).

Data analysis. Analyses were performed in MATLAB. For the behavioral experiments, hit rate was computed as $N_{hits}/(N_{hits} + N_{misses})$, where N_{hits} and N_{misses} are the numbers of hit and miss trials, respectively. FA rate = $N_{FAs}/(N_{FAs} + N_{CRs})$, and CR rate = $N_{CRs}/(N_{FAs} + N_{CRs})$, in which N_{FAs} and N_{CRs} are the numbers of FA and CR trials, respectively. The behavioral discriminability was quantified as norminv(hit rate) – norminv(FA rate), in which norminv is the inverse of the cumulative normal function[69]. For behavioral experiments in which the OFC to V1 projection was optogenetically inactivated or SST interneurons in V1 were activated, trials in laser-off and laser-on blocks in the same session were all used to compute hit rate, CR rate and discriminability.

For each trial of Go/No-Go task, we computed lick latency as the time of first lick within 1 s after stimulus onset. The lick latency in each session was quantified as the median of first lick latency across trials. For behaving mice used for V1 or OFC recordings, the lick latency (V1 recording: 476.3 ± 17.5 ms, s.e.m.; OFC recording: 447.2 ± 18.3 ms, s.e.m.) was close to 0.5 s even if the waiting period was 0.7 s. For the following analysis of neuronal responses during the waiting period, we thus used the responses within the first 0.5 s of the waiting period. To determine whether a V1 neuron was responsive to visual stimulus, we computed the baseline response during the 0.2 s before stimulus onset and the evoked firing rate during the waiting period of

stimulus presentation for each trial. Those V1 neurons in which the evoked responses during the waiting period were larger than 0.5 spike/s and were significantly higher than the baseline response ($P < 0.05$, Wilcoxon signed rank test) were used in the analysis. For the responses to No-Go stimulus during the waiting period, we divided the trials into CR and FA conditions, and computed a modulation index (MI) as $(R_{CR} - R_{FA})/(R_{CR} + R_{FA})$, in which R_{CR} and R_{FA} represented responses for CR and FA trials, respectively. For the analysis of MI, we only included neurons from those sessions in which the number of FA trials > 15. Statistical significance of the MI of each cell was determined by comparing the waiting-period responses to No-Go stimulus between CR and FA trials with Wilcoxon rank sum test. The selectivity of V1 responses to the Go and No-Go stimuli was evaluated by a selectivity index (SI), defined as $(R_{Go} - R_{No\text{-}Go})/(R_{Go} + R_{No\text{-}Go})$, in which R_{Go} and $R_{No\text{-}Go}$ are firing rates to the Go and No-Go stimuli during the waiting period, respectively.

For the experiments with optogenetic inactivation of OFC projection to V1 in behaving mice, we estimated the rate change of V1 neurons induced by laser stimulation in Go trials or No-Go trials. For Go trials, the rate change was computed as $(R_{laser\_on} - R_{laser\_off})/R_{laser\_off}$, where R_{laser_on} and R_{laser_off} represented waiting-period firing rates to Go stimulus with and without laser stimulation, respectively. For CR condition in No-Go trials, the rate change was computed as $(R_{CR\_laser\_on} - R_{CR\_laser\_off})/R_{CR\_laser\_off}$, where $R_{CR\_laser\_on}$ and $R_{CR\_laser\_off}$ represented waiting-period firing rates to No-Go stimulus in CR trials with and without laser stimulation,

respectively. For FA condition in No-Go trials, the rate change was computed as $(R_{FA\_laser\_on} - R_{FA\_laser\_off})/R_{FA\_laser\_off}$, where $R_{FA\_laser\_on}$ and $R_{FA\_laser\_off}$ represented waiting-period firing rates to No-Go stimulus in FA trials with and without laser stimulation, respectively. Because some mice had few FA trials due to a high behavioral performance, we only included V1 neurons from those sessions in which the numbers of FA trials in laser-on and laser-off conditions were both > 15.

For extracellular recordings of V1 neurons from anesthetized or awake mice not performing behavioral task, we first estimated the RFs of neurons by cross-correlating the responses with the sparse noise stimuli[70]. For the responses to oriented drifting gratings, spike rate to each stimulus was calculated by averaging the responses during the drifting period over all trials. For the responses without laser stimulation, we calculated the t statistic (mean evoked rate divided by s.e.m.) for the responses to the preferred orientation[71]. For the responses in laser-off and laser-on conditions, respectively, we computed a global measure of orientation selectivity index (OSI) as:

$$OSI = \sqrt{(\sum_i (R(\theta_i)\sin(2\theta_i)))^2 + (\sum_i (R(\theta_i)\cos(2\theta_i)))^2} \,/\, \sum_i R(\theta_i),$$

where θ_i is the angle of the drifting direction of the grating and $R(\theta_i)$ is the response at angle θ_i. Only those units with OSI > 0.08 (sensitive to orientation[72]), t > 2 (visually responsive[71]) and peak evoked firing rate > 2 Hz during laser-off condition were included in the subsequent analyses. To estimate the effect of activating OFC axons in V1 on the response amplitude of V1 neurons, we computed a rate change index as $(R_{laser\_on} - R_{laser\_off})/(R_{laser\_on} + R_{laser\_off})$, in which R_{laser_on} and R_{laser_off}

represented responses averaged over all orientations for laser-on and laser-off trials, respectively.

To identify V1-projecting OFC neurons, we used the stimulus-associated spike latency test (SALT)[55] to determine whether laser stimulation significantly changed the spike timing of neurons after stimulation onset. We also calculated Pearson's correlation coefficient between waveforms of spontaneous spikes and spikes during the 10-ms period after laser onset[73]. A unit was identified as ChrimsonR-expressing neuron if $P < 0.01$ for SALT test and waveform correlation coefficient > 0.9. To determine the response latency relative to laser onset, we binned the spikes at 0.1-ms resolution. For the peri-stimulus time histogram (PSTH) within the 10-ms period after laser onset, we identified the time of peak firing rate. For each bin of laser-evoked response within the time of peak response, we tested the difference between the firing rate in this bin and that averaged over 10-ms duration before laser onset (t test)[74]. The latency was identified as the first time point after laser onset with $P < 0.01$.

For OFC neurons recorded from behaving mice, we computed the baseline firing rates during the 0.2 s before stimulus onset and the responses to visual stimuli during the waiting period. Those neurons in which the waiting-period responses were significantly different from the baseline responses ($P < 0.05$, Wilcoxon signed rank test) were used in the analysis. We computed MI for V1-projecting OFC neurons using the same equation for V1 neurons. For OFC neurons, we also computed a response index (RI) for the responses to Go stimulus in hit trials and the responses to

No-Go stimulus in CR (or FA) trials, respectively. RI was defined as (R_{evoked} - $R_{baseline}$)/(R_{evoked} + $R_{baseline}$), where R_{evoked} and $R_{baseline}$ represented the waiting-period firing rate and the baseline rate, respectively.

For fiber photometry experiments, the value of fluorescence change ($\Delta F/F$) was derived by calculating $(F - F_0)/F_0$, where F_0 is baseline fluorescence signal averaged over 2 s before laser stimulation. For each mouse, we computed the peak of $\Delta F/F$ values after laser onset and the latency of peak $\Delta F/F$.

To examine whether the spike rate of V1-projecting OFC neurons during the waiting period in FA trials is affected by licking, we calculated the Pearson's correlation coefficient between the spike rate and lick rate in FA trials. Those sessions with > 5 FA trials in which licks occurred in the waiting period were used for this analysis. For each neuron, correlation with $P < 0.05$ was considered as significant.

The orofacial movements of the mice were analyzed using the FaceMap software (www.github.com/MouseLand/FaceMap)[75]. For each mouse, the motion energy PCs during the waiting period between laser-off and laser-on conditions were compared.

Statistical analysis. Sample sizes were similar to others used in the field. No statistical method was used to predetermine sample size. The statistical analysis was performed using MATLAB or GraphPad Prism (GraphPad Software). Wilcoxon two-sided signed rank test, Wilcoxon two-sided rank sum test, one-way repeated measures ANOVA, two-way repeated measures ANOVA, or two-way ANOVA with mixed

designed was used to determine the significance of the effect. Correlation values were computed using Pearson's correlation. Data were not collected in a blinded fashion. Unless otherwise stated, data were reported as mean ± s.e.m.

Data availability

The data that support the findings of this study are available from the corresponding author upon reasonable request.

Code availability

The data acquisition and analysis code are available from the corresponding author upon reasonable request.

References

69 Andermann, M. L., Kerlin, A. M. & Reid, R. C. Chronic cellular imaging of mouse visual cortex during operant behavior and passive viewing. *Front. Cell. Neurosci.* **4**, 3 (2010).

70 Jones, J. P. & Palmer, L. A. The two-dimensional spatial structure of simple receptive fields in cat striate cortex. *J Neurophysiol* **58**, 1187-1211 (1987).

71 Hoy, J. L. & Niell, C. M. Layer-specific refinement of visual cortex function after eye opening in the awake mouse. *J. Neurosci.* **35**, 3370-3383 (2015).

72 Xu, X., Ichida, J., Shostak, Y., Bonds, A. B. & Casagrande, V. A. Are primate lateral geniculate nucleus (LGN) cells really sensitive to orientation or direction? *Vis. Neurosci.* **19**, 97-108 (2002).

73 Cohen, J. Y., Haesler, S., Vong, L., Lowell, B. B. & Uchida, N. Neuron-type-specific signals for reward and punishment in the ventral tegmental area. *Nature* **482**, 85-88 (2012).

74 Xu, M. *et al.* Basal forebrain circuit for sleep-wake control. *Nat. Neurosci.* **18**, 1641-1647 (2015).

1163 75 Stringer, C. *et al*. Spontaneous behaviors drive multidimensional, brainwide
1164 activity. *Science* **364**, 255 (2019).

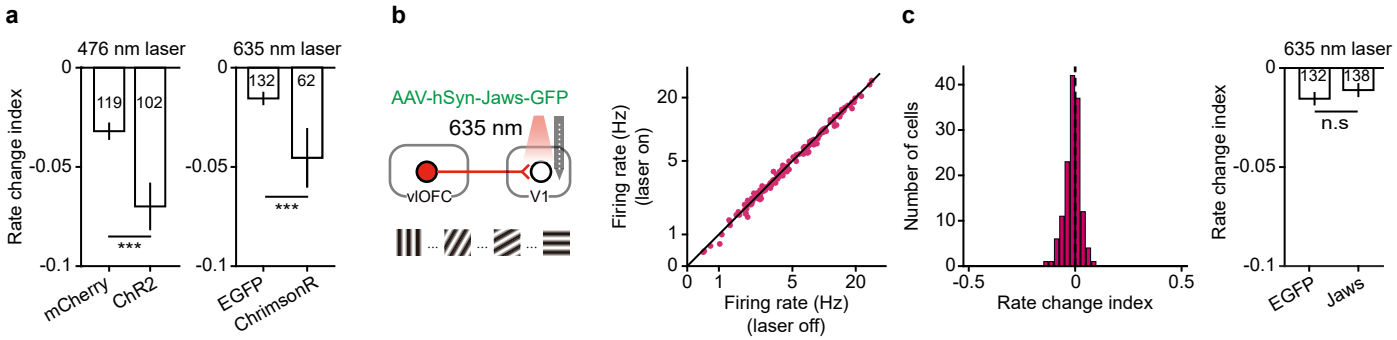

Supplementary Figure 1 | Activating OFC projection to V1 reduces response amplitude of V1 neurons, whereas inactivating OFC projection to V1 does not affect V1 response amplitude in passive-viewing mice. a, Left, comparison of rate change index of V1 neurons between mice injected with AAV-mCherry and AAV-ChR2 in the OFC. The rate change was induced by blue laser stimulation in V1. The magnitude of rate change index was significantly higher for V1 neurons in ChR2-expressing mice (n = 102 neurons) than in mCherry-expressing mice (n = 119 neurons). ***$P = 5.9\times10^{-4}$. Right, comparison of rate change index of V1 neurons between mice injected with AAV-EGFP and AAV-ChrimsonR in the OFC. The rate change was induced by red laser stimulation in V1. The magnitude of rate change index was significantly higher for V1 neurons in ChrimsonR-expressing mice (n = 62 neurons) than in EGFP-expressing mice (n = 132 neurons). ***$P = 3.9\times10^{-4}$. Wilcoxon two-sided rank sum test. **b**, Left, schematic of measuring V1 visual responses with and without inactivating OFC axons in V1. Right, mean firing rate (firing rate averaged over all orientations) of V1 neurons with laser on vs. laser off. $P = 7.4\times10^{-4}$, n = 138 neurons from awake, passive-viewing mice. **c**, Left, distribution of rate change indexes for V1 neurons shown in **b**. Right, the magnitude of rate change index was not significantly different between V1 neurons in EGFP-expressing mice (n = 132 neurons) and Jaws-expressing mice (n = 138 neurons). $P = 0.17$, Wilcoxon two-sided rank sum test. Error bars, mean ± s.e.m.

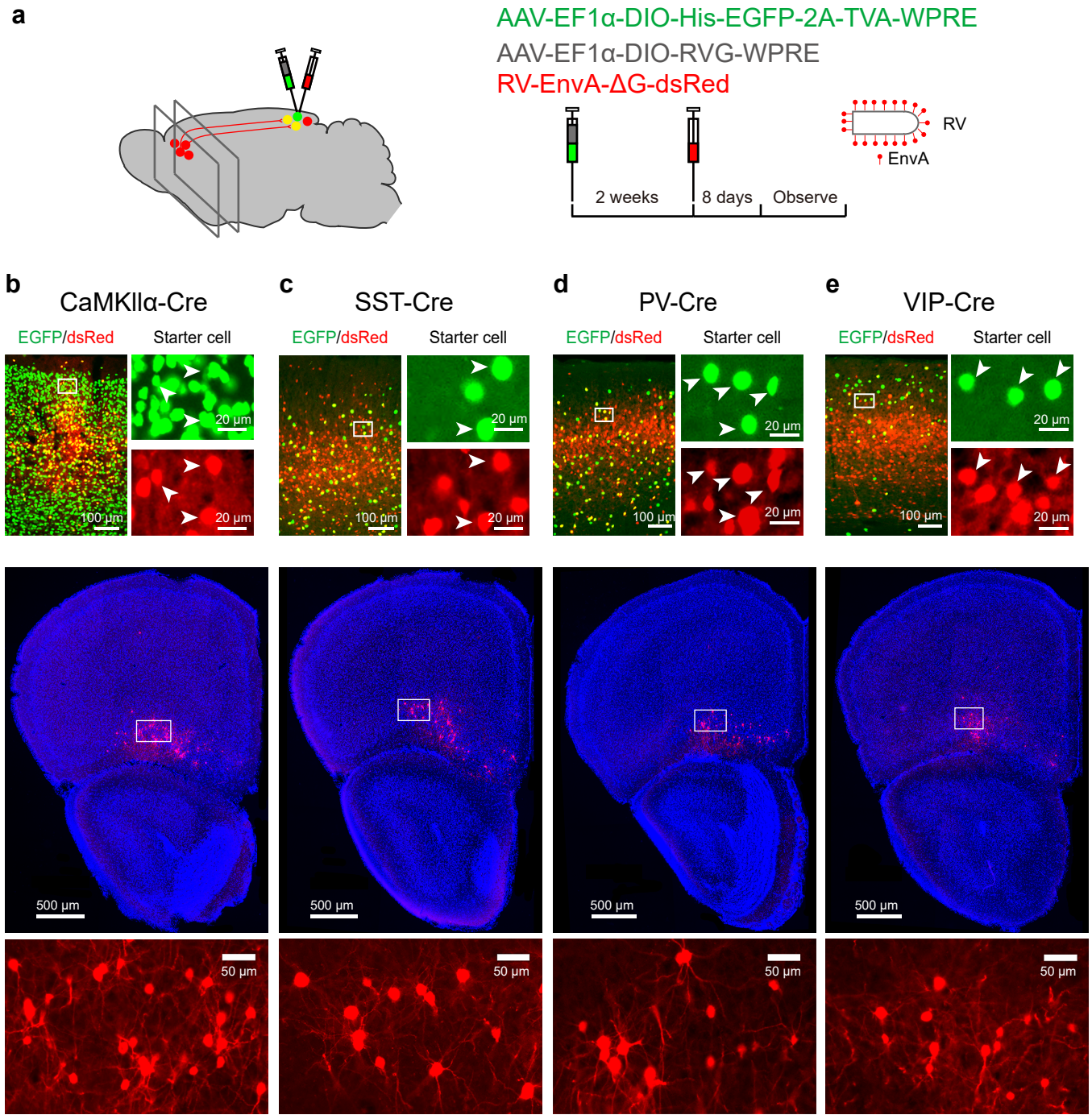

Supplementary Figure 2 | Rabies virus-mediated trans-synaptic retrograde tracing reveals monosynaptic innervation of different cell types in V1 by OFC neurons.
a, Viral injection procedure. **b**, Upper panel, injection site in V1 in a CaMKIIα-Cre mouse. Enlarged views of region in white box are shown on the right. Yellow or arrow heads, starter cells. Middle panel, fluorescence image showing trans-synaptically labeled dsRed-expressing neurons in the OFC. Enlarged view of region in white box is shown on the bottom. **c**-**e**, Similar to those described in **b** except that the images were from SST-Cre, PV-Cre and VIP-Cre mice, respectively.

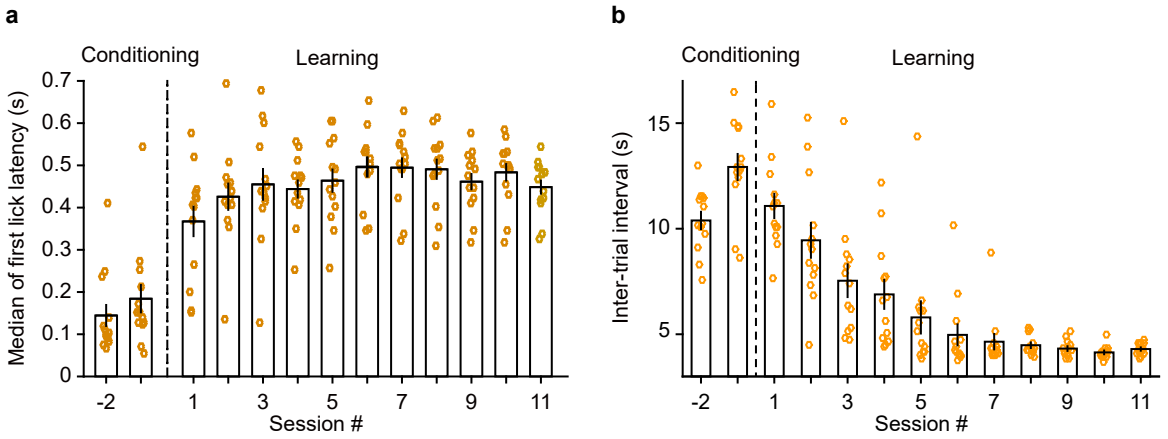

Supplementary Figure 3 | Lick latency and inter-trial interval for mice across training sessions.
a, Lick latency across sessions (2 sessions of conditioning and 11 sessions of learning the Go/No-Go task) for a population of mice ($F_{(3.03, 36.32)} = 21.81$, $P = 2.8\times10^{-8}$, $n = 13$). In each session, each circle represents the median lick latency across trials for a mouse. For each trial, lick latency was computed as the time of first lick after stimulus onset. **b**, Inter-trial interval across sessions (2 sessions of conditioning and 11 sessions of learning the Go/No-Go task) for a population of mice ($F_{(2.78, 33.37)} = 50.23$, $P = 3.76\times10^{-12}$). In each session, each circle represents the mean ITI for a mouse.

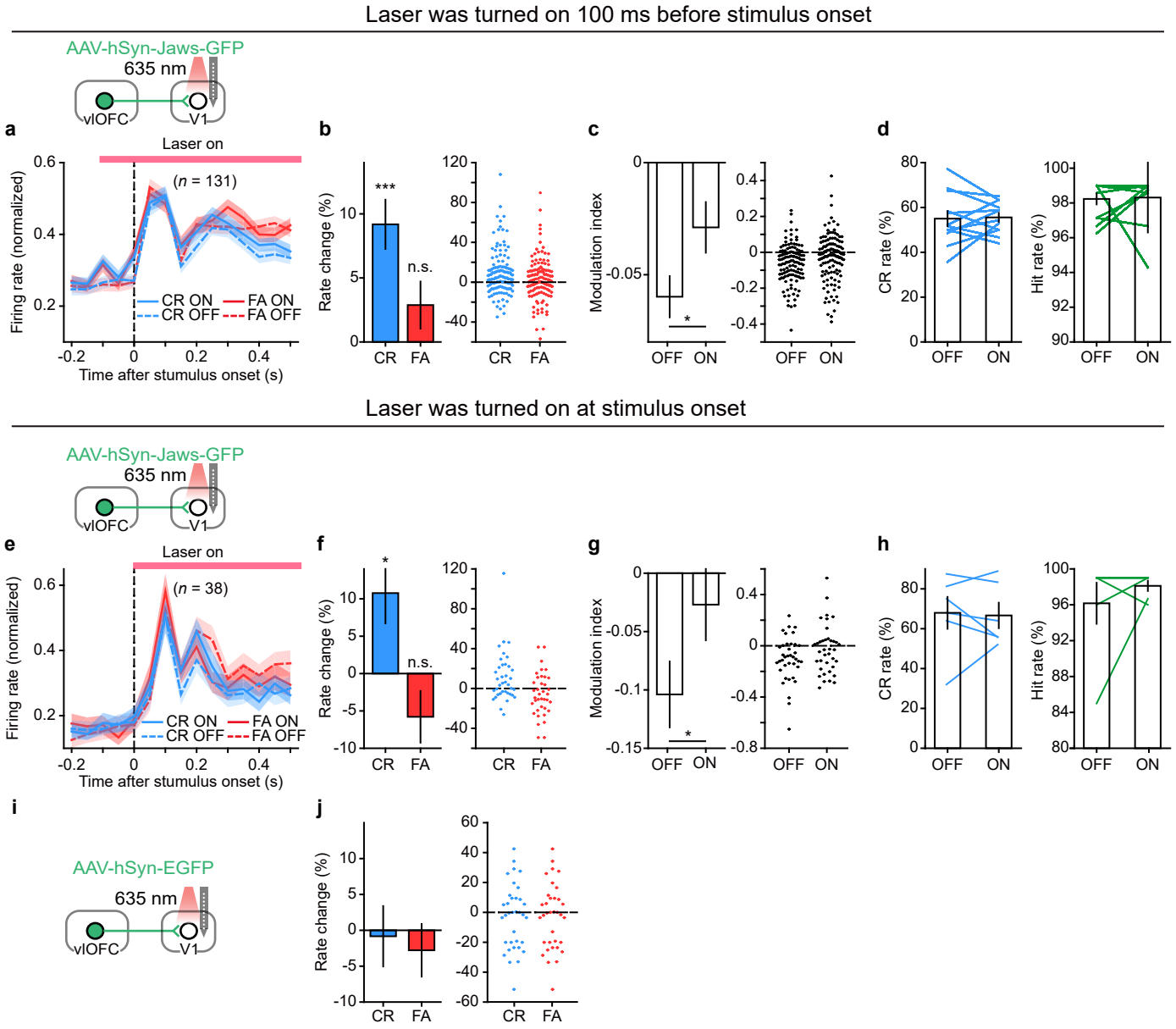

Supplementary Figure 4 | Optogenetic inactivation of OFC projection to V1 during No-Go trials increases V1 responses to No-Go stimulus in CR condition.

a-d, AAV-hSyn-Jaws-GFP was injected in the OFC. Laser stimulation in V1 during No-Go trials was turned on 100-ms before stimulus onset and covered the duration of stimulus presentation. **a**, Normalized responses to the No-Go stimulus in FA and CR trials, respectively, with and without inactivating OFC axons in V1. Horizontal line, duration of laser stimulation. **b**, Inactivating OFC axons in V1 during No-Go trials increased the responses of V1 neurons in CR (***$P = 1.7\times10^{-5}$) but not in FA trials (P = 0.12). n = 131 neurons. **c**, Inactivating OFC axons in V1 during No-Go trials significantly reduced the amplitude of MI (*P = 0.01, n = 131 neurons). **d**, Inactivating OFC axons in V1 during No-Go trials did not affect the CR rate (P = 0.91) or hit rate (P = 0.77) of the mice (n = 12 sessions from 8 mice). **e-h**, AAV-hSyn-Jaws-GFP was injected in the OFC. Laser stimulation in V1 during No-Go trials was turned on at stimulus onset and covered the duration of stimulus presentation. **e**, Normalized responses to the No-Go stimulus in FA and CR trials, respectively, with and without inactivating OFC axons in V1. Horizontal line, duration of laser stimulation. **f**, Inactivating OFC axons in V1 during No-Go trials increased the responses of V1 neurons in CR (*P = 0.02) but not in FA trials (P = 0.09). n = 38 neurons. **g**, Inactivating OFC axons in V1 during No-Go trials significantly reduced the amplitude of MI (*P = 0.01, n = 38 neurons). **h**, Inactivating OFC axons in V1 during No-Go trials did not affect the CR rate (P = 0.84) or hit rate (P = 0.75) of the mice (n = 6 sessions from 6 mice). **i**, For control mice, AAV-hSyn-EGFP was injected in the OFC. Laser stimulation in V1 during No-Go trials was turned on at stimulus onset and covered the duration of stimulus presentation. **j**, For control mice, laser stimulation in V1 during No-Go trials did not cause significant change in the responses of V1 neurons in either CR (P = 0.72) or FA trials (P = 0.53). n = 35 neurons. Data were analyzed using Wilcoxon two-sided signed rank test. Shadings and error bars denote s.e.m.

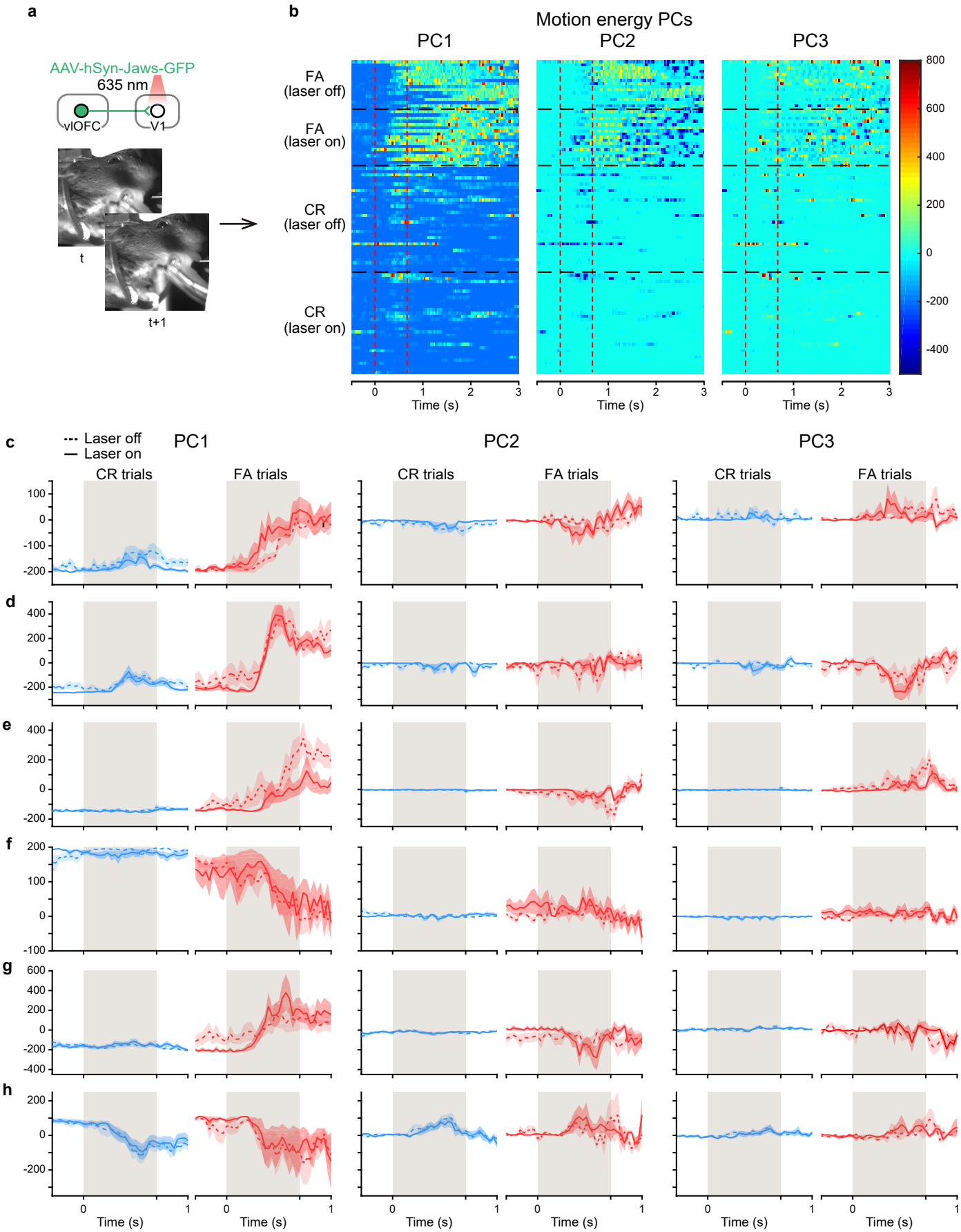

Supplementary Figure 5 | Optogenetic inactivation of OFC axons in V1 during No-Go trial did not affect orofacial movement during waiting period in CR trials.

a, Upper, strategy for inactivating OFC projection to V1 and schematic of laser stimulation. Lower, two consecutive frames from a video recording of a mouse's face during Go/No-Go visual task. **b**, The top three principle components (PCs) of the motion energy of orofacial movement in FA (CR) trials, with or without laser stimulation during No-Go trials, from an example mouse. For each PC, the time points within the two vertical dashed lines represent the waiting period. **c**, Motion energy PC averaged across trials for the mouse shown in **b**. The gray region represents the waiting period. **d-h**, Motion energy PC averaged across trials for another 5 mice. For each of these mice, motion energy PCs in CR trials during the waiting period were not significantly different between laser off and laser on conditions. $P > 0.05$, two-way repeated measures ANOVA. The mice in **c-h** were the same as those shown in **Supplementary Fig. 4h.** The orofacial movements were analyzed using the FaceMap software (www.github.com/MouseLand/FaceMap). Shadings denote s.e.m.

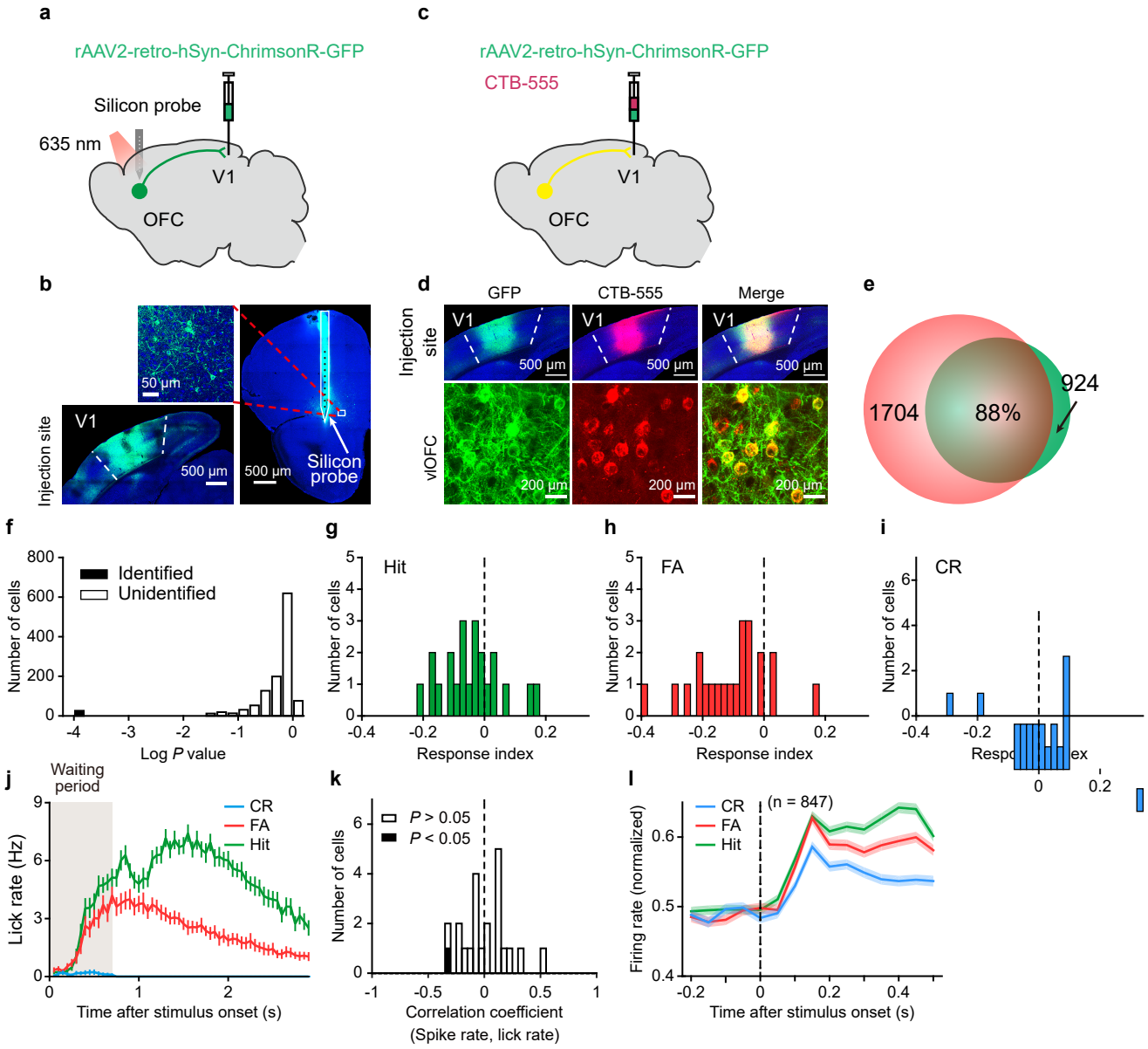

Supplementary Figure 6 | Responses of identified V1-projecting OFC neurons and unidentified OFC neurons during Go/No-Go visual task.

a, Schematic of rAAV2-retro-hSyn-ChrimsonR-GFP injection in V1 and phototagging in the OFC. **b**, Fluorescence images showing the injection site location in V1 (bottom-left), labeling of neurons in the ventrolateral OFC (vlOFC) and the electrode track marked by DiO (right). Enlarged view of region in white box is shown on the top-left. **c**, Schematic of co-injection of rAAV2-retro-hSyn-ChrimsonR-GFP and CTB-555 in V1. **d**, Fluorescence images showing the injection site location in V1 (upper) and labeling of neurons in the OFC (lower). Yellow shows the overlap of GFP and CTB signals in V1 (upper) or the OFC (lower). **e**, Percentage of OFC neurons co-labeled by GFP and CTB for the experiment shown in **c** and **d**, computed from the data of 3 mice. **f**, Histogram of log *P* values (derived from the SALT test) for 1175 OFC neurons recorded in the phototagging experiments. **g-i**, Distributions of response indexes (RIs) for identified V1-projecting OFC neurons ($n = 22$) in hit (**g**), FA (**h**) and CR (**i**) trials. The RI was defined as $(R_{evoked} - R_{baseline})/(R_{evoked} + R_{baseline})$, where R_{evoked} and $R_{baseline}$ represented the waiting-period firing rate and the baseline firing rate, respectively. The RIs in hit and FA trials were both significantly smaller than zero ($P = 0.03$ and 6.9×10^{-4}, respectively, Wilcoxon two-sided signed rank test). The RI in CR trials was not significantly different from zero ($P = 0.49$, Wilcoxon two-sided signed rank test). **j**, PSTH (50 ms/bin) of licking behavior in the waiting period and the answer period for hit, FA, and CR trials, respectively ($n = 16$ mice). The gray region indicates the waiting period. **k**, Distribution of Pearson's correlation coefficients between the spike rate of V1-projecting OFC neurons and lick rate in FA trials during the waiting period. The distribution of correlation was not significantly different from zero ($P = 0.96$, $n = 22$, Wilcoxon two-sided signed rank test). **l**, The responses of unidentified OFC neurons in the Go/No-Go task. The responses of each neuron were normalized by peak response across hit, FA and CR conditions, and were averaged across all neurons ($n = 847$). The responses in FA trials were significantly higher than those in CR trials. $F_{(1, 846)} = 43.35$, $P = 8.0\times10^{-11}$, two-way repeated measures ANOVA. Shadings and error bars, mean ± s.e.m.

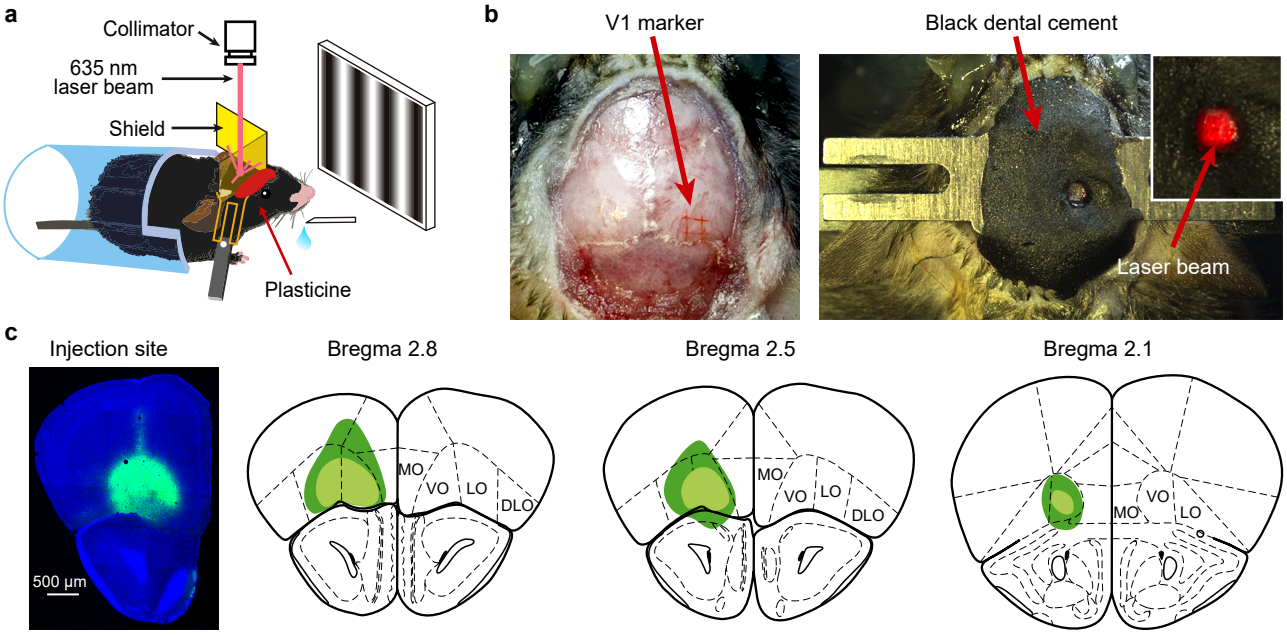

Supplementary Figure 7 | AAV-Jaws was expressed in the OFC of mice performing Go/No-Go visual task. **a**, Images of behavioral setup and optogenetic manipulation. **b**, Left, the skull region above V1 was marked during the surgery; Right, after virus injection in the OFC the headplate was fixed to the skull using dental cement mixed with carbon powder. The cement covered the skull except the region above V1 so that photostimulation of area beyond V1 was prevented. Inset, V1 region was stimulated with red laser. **c**, Left, fluorescence image showing the expression of AAV-CaMKIIα-Jaws-GFP in the OFC in a C57BL/6 mouse. Right, the maximal (green) and minimal (light green) extent of virus expression in the OFC for all Jaws-expressing mice in **Fig. 6.**

Supplementary Video 1 | Example of orofacial movements from trials with and without optogenetic inactivation of OFC projection to V1.

The mouse was performing a Go/No-Go visual task. The session consisted of interleaved blocks of laser-on and laser-off trials. In laser-on blocks, laser stimulation was applied to V1 during No-Go trials to inactivate the OFC projection to V1. The video shows a hit trial, two FA trials (laser-off and laser-on), and two CR trials (laser-off and laser-on). ITI, inter-trial interval.